First metatarsal trabecular bone structure in extant hominoids and Swartkrans hominins.

Klara Komza [1,2], Matthew M. Skinner [2,3]

[1] Department of Anthropology, University of Toronto, Canada

[2] School of Anthropology and Conservation, University of Kent, Canterbury, United Kingdom

[3] Department of Human Evolution, Max Planck Institute for Evolutionary Anthropology, Leipzig, Germany

Corresponding author:
Klara Komza
Department of Anthropology
University of Toronto
19 Russell St.
Toronto, ON
M5S 2S2
Phone: +1(647)393-8644

Abstract

Changes in first metatarsal (MT1) morphology within the hominin clade are crucial for reconstructing the evolution of a forefoot adapted for human-like gait. Studies of the external morphology of the MT1 in humans, non-human apes and fossil hominins, have documented changes in its robusticity, epiphyseal shape and its articulation with the medial cuneiform. Here, we test whether trabecular structure in the MT1 reflects different loading patterns in the forefoot across extant large apes and humans, and within this comparative context, infer locomotor behaviour in two fossil hominins from Swartkrans, South Africa. Microtomographic scans were collected from the MT1 of *Pongo* sp. (n=6), *Gorilla gorilla* (n=10), *Pan troglodytes* (n=10), *Homo sapiens* (n=11), as well as SKX 5017 (*Paranthropus robustus*), and SK 1813 (Hominin gen. sp. indet.). Trabecular structure was quantified within the head and base using a 'whole-epiphysis' approach with medtool 4.2. We found that modern humans displayed relatively higher bone volume fraction (BV/TV) in the dorsal region of each epiphysis and a higher overall degree of anisotropy (DA), whereas great apes showed higher BV/TV in the plantar regions, reflecting dorsiflexion at the metatarsophalangeal (MTP) joint in the former and plantarflexion in the latter. Both fossils displayed low DA, with SKX 5017 showing a hyper-dorsal concentration of trabecular bone in the head (similar to humans), while SK 1813 showed a more central trabecular distribution not seen in either humans or non-human apes. Additionally, we found differences between non-human apes, modern humans, and the fossil taxa in trabecular spacing (Tb.Sp.), number (Tb.N.), and thickness (Tb.th.). While low DA in both fossils suggests increased mobility of the MT1, differences in their trabecular distributions could indicate variable locomotion in these Pleistocene hominins (recognizing that the juvenile status of SK 1813 is a potential confounding factor). In particular, evidence for consistent loading in hyper-dorsiflexion in SKX 5017 would suggest locomotor behaviours beyond human-like toe off during terrestrial locomotion.

Keywords: trabecular bone, *Paranthropus*, locomotion, bipedalism

1. Introduction[1]

One of the central questions within the study of human evolution is how and when obligate bipedalism emerged. The forefoot is of particular importance in addressing this question because it directly reflects the extent to which a species uses its feet for locomotion (either arboreal or terrestrial) and/or manipulation. The first metatarsal (MT1) has undergone a dramatic transformation, from a digit used primarily for grasping, to a digit used mainly for weight-bearing, stabilization, and propulsion in modern humans (Morton, 1922; Elftman and Manter, 1935; Susman, 1983; Harcourt-Smith and Aiello, 2004). Analysis of the partially preserved OH 8 foot formed a critical aspect of the initial diagnosis of bipedalism in *Homo habilis* (Day and Napier, 1964; Kidd et al., 1996) and a number of studies have incorporated analyses of forefoot bones to argue for committed terrestrial bipedalism in *Australopithecus afarensis* (Latimer and Lovejoy, 1990; ; Ward 2002 Ward et al., 2011) and an opposable hallux in *Ardipithecus ramidus* (Lovejoy et al., 2009; White et al., 2015). Equally intriguing is the recent discovery of the Burtele foot, which is similar in age to *A. afarensis* but displays a number of characteristics that differentiate it morphologically and suggest two different types of bipedal foot loading in the hominin clade at the same time (Haile-Selassie et al., 2012). This variation in hominin foot bone morphology highlights the importance of understanding the form/function relationship of the MT1 in extant and fossil hominoids and, in particular, whether internal bone structure can provide insights into biomechanical loads experienced by the foot during different types of locomotion. Using a comparative sample of modern humans and non-human apes, this study will address whether trabecular structure within the MT1 is reflective of locomotor mode. Furthermore, we will compare them to fossil hominins from Swartkrans (SKX 5017 and SK 1813) to test hypotheses about hominin locomotion in the Plio-Pleistocene of South Africa.

1.1. Bone functional adaptation

Functional interpretations of fossil hominin locomotion largely vary because of a lack of consensus on the functional significance of various external skeletal features. It remains unclear whether 'primitive' features represent non-functional evolutionary vestiges, or if they represent

[1] Abbreviations: metatarsophalangeal (MTP); tarsometatarsal (TMT)

functional indicators of locomotor behaviour (Stern and Susman, 1983; Clarke and Tobias, 1995; Ward, 2002; Harcourt-Smith and Aiello, 2004; Zipfel et al., 2009). This issue can be partially addressed by studying aspects of bone that are more responsive to external loading. While articular surfaces indicate the joint positions an element is capable of, internal bone is more likely to show the position in which the element was actually loaded (Ruff and Runestad, 1992; Rafferty and Ruff, 1994; Jacobs, 2000; Rubin et al., 2002; Ruff et al., 2006). Diaphyseal cortical bone has been shown to respond to mechanical stress in the shaft and can be indicative of predominant bending forces experienced during loading (Ruff, 1983; Cowin et al., 1985; Doden, 1993; Carlson, 2005; Ruff et al., 2006). However, its function is likely different over joint articular surfaces, where it becomes significantly thinner. It is also covered by cartilage and often contained within a synovial joint. Conversely, the trabecular bone located subchondrally within epiphyses remodels at a faster rate than cortical bone (Eriksen, 2010), and can provide evidence of in vivo loading that may be more useful at reconstructing predominant joint position and associated behaviors (Hodgskinson and Currey, 1990; Rubin et al., 2002; Mittra et al., 2005; Pontzer et al., 2006; Barak et al., 2011; but see Bertram and Swartz, 1991). However, it should be noted that trabecular bone structure does not always correlate with known locomotor patterns in certain mammals, including mice and several primates (Carlson et al., 2008; Ryan and Walker, 2010; Shaw and Ryan, 2012).

The current study focuses on two main structural properties of trabecular bone: bone volume fraction (BV/TV), which is a measure of trabecular thickness, number, and spacing, and degree of anisotropy (DA), which reflects the degree to which trabecular struts are oriented in the same direction. These parameters account for 87-89% of the variance in the strength of a bone (Young's modulus) (Maquer et al., 2015), have been shown to change in relation to magnitude, frequency, and direction of load in in vivo studies (Lanyon, 1974; Hodgskinson and Currey, 1990; Biewener et al., 1996; Mittra et al., 2005; Pontzer et al., 2006; Barak et al. 2011), and to differ among taxa that employ different modes of locomotion (MacLatchy and Müller, 2002; Ryan and Ketcham, 2002, 2005; Ryan and Shaw, 2012; Scherf et al., 2013; Tsegai et al., 2013, 2017; but see Fajardo et al., 2007; Ryan and Walker, 2010). BV/TV and DA are informative parameters because both are less likely to scale allometrically and have been found to respond to loading in predictable ways. BV/TV is generally

higher in areas that experience greater compressive loading, and trabecular orientation adapts to the main axis of joint movement (Biewener et al., 1996; Guldberg et al., 1997; Ryan and Ketcham, 2002; Mittra et al., 2005; Pontzer et al., 2006; Chang et al., 2008; Polk et al., 2008; Harrison et al., 2011; Saparin et al., 2011). Responses in DA and BV/TV to biomechanical stressors have been demonstrated in several classic studies on the mammalian calcaneus (Lanyon, 1973, 1974; Skerry and Lanyon, 1995; Biewener et al., 1996; Skedros et al., 2004, 2012; Sinclair et al., 2013). In animals in which the calcaneus does not touch the ground during locomotion, trabeculae underlying the Achilles tendon were aligned with the compressive and tensile principal direction of stress (Lanyon, 1974; Biewener et al., 1996). When external loading was removed by detaching the calcaneal tendon, BV/TV reduced as a result of lower trabecular thickness and number (Biewener et al., 1996). Further in vivo studies have supported this. Barak et al. (2011) showed that DA and BV/TV varied predictably in the distal tibiae of sheep that loaded their ankles in different positions. Pontzer et al. (2006) also found strong correlations of DA with changes in external loading at the distal femur of guinea fowl.

However, there are several non-mechanical factors that may affect trabecular structure. It is not clear how genetic, hormonal, and environmental factors constrain its structure (Simkin et al., 1987; Judex et al., 2009; Havill et al., 2010; Devlin, 2011; Devlin and Bouxsein, 2012; Devlin et al., 2013), how its response varies based on frequency versus magnitude of mechanical loading (Skerry and Lanyon, 1995; Lambers et al., 2013), as well as anatomical region (Räth et al. 2013; Wallace et al., 2013). Furthermore, by measuring trabecular bone density throughout 9 anatomical regions in humans, Chirchir (2016) found that most sites have homogenous values, suggesting they are influenced by site-specific genetic factors. Nonetheless, computational models (Odgaard et al., 1997; Huiskes et al., 2000; Fox and Keaveny, 2001) and in vivo studies (Lanyon, 1974; Biewener et al., 1996; Pontzer et al., 2006; Barak et al., 2011) have demonstrated strong links between trabecular structure and the frequency, magnitude, and direction in which a joint is loaded.

1.2. Biomechanics of the first metatarsal

Modern humans are adapted for a bipedal mode of locomotion and possess a forefoot structure in which each metatarsophalangeal (MTP) joint acts as a weight bearing and propulsive

139 structure during the push-off part of the stance phase (Stokes et al.,1979; Christensen and Jennings,
140 2009; Griffin et al., 2015). During this phase, the MTP joints dorsiflex, moving the proximal
141 phalanges on to the dorsum of their respective metatarsal heads. This causes tightening of the plantar
142 aponeurosis, stabilizing the foot and elevating the longitudinal arch, which changes its conformation
143 to a stiff lever for propulsion and ultimately toe-off (Hicks, 1954; Bøjsen-Moller, 1979; Susman,
144 1983; Caravaggi et al. 2010; Griffin et al., 2015). As shown by in vivo studies of plantar pressure
145 distribution within the human foot, during dorsiflexion the medial forefoot shows a spike in loading
146 (Hutton and Dhanendran, 1981; Katoh et al., 1983; Soames, 1985; Munro, 1987; Lee and Farley,
147 1998; Hunt et al., 2001; Nester et al., 2007; Griffin et al., 2010a). The MT1 bears a large portion of
148 this load and this is reflected by its large head, which experiences high compressive forces during
149 push-off (Rodgers, 1995; Donahue and Sharkey, 1999; Vereecke et al., 2003; D'Août et al., 2004). Its
150 external shape is also designed to stabilize the MTP joint and facilitate dorsiflexion during push-off.
151 The superior aspect of the articular surface of the head expands to the dorsum of the bone, resulting in
152 a raised appearance in relation to its shaft, which is thought to increase the range of dorsiflexion at the
153 MTP joint (Stokes et al., 1979; Susman and Brain, 1988; Susman and de Ruiter, 2004; Griffin and
154 Richmond, 2005; Griffin et al., 2010a). It is also medio-laterally wider on the dorsal aspect of the
155 head than the plantar aspect, which has been argued to enhance joint stability during push-off and
156 facilitate close-packing of the MTP joint (Susman and Brain, 1988; Hetherington et al., 1989; Susman
157 and de Ruiter, 2004; Pontzer et al., 2010, Fernández et al., 2015).
158 Analyzing foot kinematics in extant non-human apes is less straight-forward compared to
159 modern humans because they employ a wider range of locomotion, from terrestrial to arboreal
160 quadrupedalism, vertical climbing, suspension, and occasional terrestrial bipedalism. However, in
161 vivo studies of chimpanzee and bonobo footfall patterns show considerable differences from modern
162 humans (Aerts et al., 2000; Vereecke et al., 2003; D'Août et al., 2004; Griffin et al., 2010a;
163 Wunderlich and Ischinger, 2017). During terrestrial quadrupedal locomotion, bonobos show a higher
164 spike in loading on the lateral aspect of the foot during push-off, with relatively little force inflicted
165 upon the MT1 (Vereecke et al., 2003). Additionally, during vertical climbing, chimpanzees show peak
166 loading under the medial metatarsals, when the MTP joints are plantarflexed (Wunderlich and

Ischinger, 2017). If these plantar pressure patterns can be broadly applied to non-human apes, they would suggest that the first MTP joint incurs maximum loading when it is used for grasping.

This is reflected within the shape of the MT1 head, which in all non-human apes is mediolaterally expanded on the plantar aspect (Susman, 1983; Latimer and Lovejoy, 1990; Marchi, 2005, 2010; Griffin and Richmond, 2010; Fernández et al., 2015). The same mechanism that allows for close-packing of the MTP joint during dorsiflexion in humans allows for close-packing during plantarflexion in non-human apes, increasing stability during pedal grasping (Susman, 1983; Griffin et al., 2010a). It should be noted that within non-human apes, there is variation in how the hallux is used for locomotion. Although comparative plantar pressure distribution data for *Gorilla* and *Pongo* do not exist, a substantial amount of information can be obtained through observational studies (Tuttle and Beck, 1972; Cant, 1987; Sarmiento, 1994; Remis, 1995; Gebo, 1996; Doran, 1997; Sarringhaus et al., 2014), skeletal (Susman, 1979; Shea, 1981; Inouye, 1992; Doran, 1993; Marchi, 2005; Richmond, 2007; Congdon, 2012; Drapeau and Harmon, 2013; Jashashvili et al. 2015), and soft tissue morphological analyses (Oishi et al., 2012). Such studies show different habitual positioning of the hallux; orangutans generally do not apply significant force on the hallux during suspension, whereas chimpanzees generally do (Oishi et al., 2012). Gorillas do not use their feet for suspension; when they locomote arboreally, their size restricts them to substrates of larger diameters. Their feet are used for vertical climbing or walking, but because the supports they use for climbing are usually large relative to their foot size, there is little flexion of the metatarsophalangeal and interphalangeal joints (Sarmiento, 1994; Remis, 1995).

The proximal articular surface of the MT1 is equally reflective of locomotor behavior. Within modern humans, it is relatively broad and flat, corresponding to a stable tarsometatarsal (TMT) joint complex that reduces mediolateral mobility of the hallux, and keeps it in line with the other metatarsals (Morton, 1924; Susman and Brain, 1988; Proctor et al. 2008; Proctor, 2010; Gill et al. 2015). Its broad mediolateral width is related to the bending stresses experienced near the base of the MT1, and its increased cross-sectional area is a response to high compressive forces at the joint and high tensile forces inflicted upon the ligaments (Stokes et al., 1979; Griffin and Richmond, 2005). In all other living great apes, the proximal MT1 does not experience such high loading, resulting in a

proximal surface that has a smaller overall area. The TMT joint is instead adapted for a wider range of movement associated with grasping and varied locomotion. The proximal articular surface of the MT1 is concave, and the distal articular surface of the medial cuneiform is convex, allowing for multiaxial movement of the hallux that is more effective for climbing and grasping (Latimer and Lovejoy, 1990; McHenry and Jones, 2006; Tocheri et al., 2011).

1.3. Early hominin locomotion

Here, we focus specifically on Plio-Pleistocene fossil feet from South Africa, which show a diverse range of morphological features. StW 573, attributed to *Australopithecus prometheus* (but see Berger and Hawks, 2019), shows evidence of a slightly divergent hallux and has been interpreted as adept at tree-climbing (Clarke and Tobias, 1995; Clarke, 2013) but see (Harcourt-Smith et al., 2002). Two isolated MT1s from Sterkfontein (StW 562 and StW 595) suggest there was locomotor diversity in South African hominins. The two metatarsals are of unknown taxonomic status but were both found in Member 4, dated between 2.6 and 2.0 mya (Pickering and Kramers, 2010), and show striking differences in external morphology. StW 562 is described as more human-like based on its distal epiphysis which shows dorsal doming of the head, and because it is relatively robust. StW 595 is relatively gracile and does not show this epiphyseal feature, suggesting this individual had a more ape-like push-off mechanism (Clarke, 2013; DeSilva et al., 2019). Of particular relevance to this study are the postcranial remains of South African robust australopiths attributed to *Paranthropus robustus*. *P. robustus* is mainly represented by cranial remains (Grine, 1993; Grine and Daegling, 1993; Wood and Constantino, 2007); postcranial remains are relatively abundant, but cannot be attributed with complete confidence to the taxon. Based on pelvic, femoral, and tarsal morphology, the gait of *P. robustus* has been described as bipedal, but with a 'waddling gait' and a less efficient body weight transfer mechanism (Napier, 1964; Day and Napier, 1965; Robinson, 1972; Gebo and Schwartz, 2006). However, trabecular properties of the talus (Su and Carlson, 2017) and diaphyseal cortical bone morphology of the fifth metatarsal (Dowdeswell et al., 2017) suggest a medial weight transfer of the foot during push-off and loading of the lateral column in a human-like way.

Two complete metatarsals from Swartkrans contribute to our understanding of Early Pleistocene hominin locomotion. SKX 5017 is an isolated left MT1 recovered from the Lower Bank

deposit of Swartkrans Member 1, dated to approximately 1.5-1.8 mya (Susman and Brain, 1988; Susman and de Ruiter, 2004). Along with other fossils found within this level, SKX 5017 is attributed to *P. robustus*. The specimen is described as short and similar in length to OH 8 and female bonobos (Susman and Brain, 1988). The base of the metatarsal has a mildly concave and ovoid shape, similar to modern great apes (Susman and Brain, 1988), although the morphology of the base and proximal shaft provide evidence that human-like plantar ligaments (and perhaps an aponeurosis) were present. Based on this basal articular morphology, and on the degree of torsion between the head and the base, there is no indication that the hallux was abducted to an ape-like degree (Susman and Brain, 1988). The head displays a mosaic of primitive and derived features. The superior articular surface of the head extends onto the dorsum of the shaft, which is an indication of increased dorsiflexion at the MTP joint. In contrast, the dorsal medio-lateral breadth of the head is narrower than the plantar breadth, suggesting the joint did not close-pack in dorsiflexion, and thus was less stable during push-off (Susman and Brain 1988).

SK 1813 is a nearly complete right MT1 found in a backfill hole of Swartkrans and is thought to have come from Member 1 or 2, but attribution to a specific stratigraphic unit or taxon cannot be made with certainty (Susman and de Ruiter, 2004). Presence of an epiphyseal line near the base signals the subadult status of this individual, with an estimated age of approximately 15 years (Susman and de Ruiter, 2004). It bears strong morphological affinities to SKX 5017, albeit the former is smaller. It has the same dorsal mediolateral narrowing on the head, and expansion of the dorsal articular surface onto the dorsum of the shaft. The base is also dorsoplantarly expanded, which is reflective of increased tensile forces from well-developed plantar ligaments in response to a bipedal gait (Susman and de Ruiter, 2004; Proctor et al. 2008; Proctor, 2010). The shape of the proximal articular surface is difficult to discern due to post-mortem damage, but is nonetheless described as concave and ovoid, typical of non-human apes (Susman and de Ruiter, 2004). In this study, we examine trabecular structure within the epiphyses of these two specimens to reconstruct aspects of their biomechanical loading regime and in doing so make inferences about the locomotor behaviours of the individuals they represent.

1.4. Previous trabecular analysis of the MT1

252 Predictions about how mechanical loading affects the trabecular bone within the MT1 can be
253 made a priori based on currently-known patterns within the MT1 head of *Homo sapiens*, *Pan*
254 *troglodytes*, *Pan paniscus*, and *Gorilla gorilla* (Griffin et al., 2010b). Volume of interest (VOI)-based
255 analysis has shown that modern humans exhibit significantly higher DA values than non-human apes,
256 consistent with a tightly constrained joint with a relatively uniaxial range of movement. The same
257 study has shown BV/TV to be less effective at differentiating locomotor behavior between species,
258 but this may be caused by the methodological limitations of using VOIs in analyzing trabecular
259 structure. Overall, these results suggest that among trabecular bone properties, a high degree of
260 anisotropy is the most indicative factor of a forefoot habitually used for propulsion during bipedal gait
261 (Griffin et al. 2010b).

262 *1.5. Aims and predictions*
263
264 Based on known loading patterns within the forefoot of modern humans and great apes, and the
265 mechanical adaptations of trabecular bone, we test the following hypotheses:

266 1. Modern humans will have a higher BV/TV within the dorsal aspect of the MT1 head and
267 base, and non-human apes will display the opposite pattern. This corresponds to the position
268 in which the joints close-pack and incur the highest compressive load.
269 2. Modern humans will show higher overall DA and non-human apes will show lower overall
270 DA within the entire element, corresponding to the range of motion at the TMT joint and the
271 MTP joint. We also predict that modern humans will show relatively higher DA in the dorsal
272 regions of the epiphyses compared to the non-human apes.
273 3. Based on their external morphology, we hypothesize that SKX 5017 and SK 1813 will show
274 similar trabecular distribution to modern humans. However, because of a more concave and
275 rounded proximal articular facet in SKX 5017 indicative of a relatively mobile joint, its base
276 will have a lower DA than modern humans.

277 To ensure no confounding factors relating to body size, we also test for interspecific allometry in
278 trabecular bone variables. Following the results of previous studies on the talus and tibia of modern
279 humans and chimpanzees (Tsegai et al., 2017), and on the lower limbs of modern humans (Saers et al.

2016), we predict that there will be no significant allometric scaling between any trabecular parameter and bone size. Furthermore, because Tsegai et al. (2017) found that the tibia and talus do not show the same patterns of scaling in regards to Tb.Th., BV/TV, or DA, we expect that the MT1 will also display allometric patterns not displayed in either element.

2. Methods

2.1. Sample

The comparative sample consists of thirty-nine MT1s from modern non-human apes and modern humans: six *Pongo* sp., ten *Gorilla gorilla*, ten *Pan troglodytes*, and eleven *Homo sapiens.* Details of the study sample are shown in **Table 1**. Orangutans were wild-shot, but their provenance is unknown, with the exception of one captive male from the Munich Zoo. Gorillas were all wild-shot in Cameroon and the French Congo. Some chimpanzee specimens were collected from the Taï National Park, Republic of Côte d'Ivoire; others were wild-shot in Cameroon. The modern human sample was composed of likely sedentary and shod individuals from two 19^{th}-20^{th} century cemeteries in Göttingen, Germany (for more information on the comparative sample, see SI, Table S1). Specimens were chosen if the individuals were adult, free from signs of pathology, and if their trabecular bone was well-preserved. Adult status was determined based on external morphology of the associated postcrania and dental eruption. Additional information on individual specimens is provided within the supplemental online information. Two fossil hominin MT1s were obtained from the Ditsong National Museum of Natural History and derive from the site of Swartkrans, South Africa. One is attributed to *Paranthropus robustus* (SKX 5017), and the other being of unassigned taxonomic status (SK 1813). SKX 5017 is complete and well-preserved, but because of extensive cortical and trabecular damage to the base of SK 1813, only the head was analyzed.

2.2. Image Acquisition

Specimens were scanned at the Max Planck Institute for Evolutionary Anthropology in Leipzig and at Cambridge University. The modern *Homo* and *Pongo* specimens were scanned using a Diondo d3 high-resolution micro-CT system in Leipzig with an acceleration voltage of 140 kV, and 120 µA and 140 µA respectively, using a 0.5 mm brass filter. The images were reconstructed as 3000 x 3000 16 bit tiff image stacks from 3240 projections with two frame averaging. The Taï Forest *Pan*

troglodytes sample was scanned using a Skyscan 1173 with an acceleration voltage of 100 kV and 62 µA using a 1.0 mm aluminium filter. The images were reconstructed from 2240 x 2240 16 bit tiff image stacks from 2400 projections with two frame averaging. *Gorilla gorilla* and *Pan troglodytes* specimens from the Powell-Cotton Museum were scanned using a Nikon Metrology XT H 225 ST High resolution CT scanner in Cambridge University. They were scanned at an acceleration voltage of 135 kV and 135 µA with no filter. The images were reconstructed as 2000 x 2000 16 bit tiff image stacks from 1080 projections with one frame averaging. All specimens were scanned with an isometric voxel resolution between 27 and 42 µm.

2.3. Specimen segmentation

Scans were segmented into binary format using the Ray Casting Algorithm (RCA) (Scherf and Tilgner, 2009). This method is most effective where there is clear separation between bone and air, and where there is little matrix within the epiphysis. All extant taxa, along with SKX 5017 were segmented using this method. Due to a large amount of matrix within the epiphysis of SK 1813, it was segmented using a machine learning clustering algorithm that is most effective where there is matrix that falls within the greyscale range of trabecular bone (Dunmore et al., 2018). This algorithm assigns voxels in an image to one of three predefined classes, based on the probability that its greyscale value would be in each class. Therefore, it allows for segmentation of problematic areas that the RCA does not handle effectively.

2.4. Medtool

The segmented images were processed through a customized script within medtool v4.2 (www.dr-pahr.at), a python-based script manager. Each step of this method has been described by Pahr and Zysset (2009) and tested by Gross et al. (2014). Using the segmented image (**Fig. 1a**), the outer surface (**Fig. 1b**), and inner surface (**Fig. 1c**) were defined and subtracted from one another to create an image of the cortex only (**Fig. 1d**). An image of the trabecular bone (**Fig. 1e**) only was obtained by subtracting the cortex image from the original segmented image. A series of mask overlays were created to separate the cortical and trabecular bone, and 'inside air' from 'outside air' by assigning them to different grey values (**Figs. 1f, g, h**). A 3D mesh of the mask images was

obtained using the computational geometry algorithms library (CGAL version 4.10, Computational Geometry, http://www.cgal.org), a mesher that creates a 3D finite element model using 3D Delauney triangulation (Delaunay, 1934). Trabecular bone was analyzed through the placement of multiple spherical VOIs onto a rectangular background grid of 2.5 mm grid spacing over the MaskSegIn image (**Fig. 1f**). VOIs were placed at each node with a set diameter of 5 mm to ensure overlap. Trabecular parameters were measured within each VOI, and values were assigned to each grid node. These values were then interpolated to the tetrahedral elements, resulting in BV/TV and DA color maps that were visualized using Paraview 3.14.1 (Sandia Corporation, Kitware. Inc).

Within each VOI, bone volume fraction (BV/TV) was calculated as the ratio of bone voxels to bone and air voxels. The trabecular orientation (second rank fabric tensor) was calculated using the Mean Intercept Length (MIL) method (Whitehouse, 1974; Odgaard, 1997). This gave results for first, second, and third eigenvectors and eigenvalues. Fabric degree of anisotropy (DA) was calculated as (1 – [eigenvalue 3/eigenvalue 1]), resulting in numbers from 0 to 1 (representing complete isotropy and anisotropy, respectively). The values within each VOI were averaged to obtain results for the entire section. In addition to BV/TV and DA, trabecular thickness (Tb.th., mm), trabecular number (Tb.N, mm^{-1}), and trabecular spacing (Tb.S, mm) were calculated within each VOI.

2.5. Statistical analysis

Because the focus of this research is on trabecular bone structure, statistical analysis was confined to the epiphyses; the shaft, which contains little to no trabeculae was separated from the head and base. In each scan, the head was separated where the articular surface on the plantar aspect terminated, as it is clearly delineated from the shaft. When viewing the element in plantar view, each metatarsal displays a pronounced curvature on the proximal and medial aspect of the shaft. The cut for the base was made where this curvature was most pronounced (**Fig. 2a)**. The base and the head were further separated into dorsal and plantar regions by taking their maximum dorso-plantar length and dividing it by half (**Fig. 2b**).

Statistical analysis was performed using RStudio v1.0.153 (RStudio Inc. 2015), and plots were generated using ggplot2 (Wickham, 2009). All trabecular variables were tested for allometry

using reduced major axis regression, through the R package lmodel2 (Legendre, 2018). Because data for body size was unavailable for the study sample, the geometric mean for each specimen was used as a proxy for body size. This was calculated using five linear measurements of the metatarsal as proposed by De Groote and Humphrey (2011), which included maximum MT1 length, as well as dorsoplantar and mediolateral length of the proximal and distal articular surfaces.

Standard non-parametric tests were used because of small sample sizes, and because not all regions in all taxa showed a normal distribution. Pair-wise comparisons using Mann-Whitney U tests were conducted to investigate intraspecies differences in BV/TV and DA between the dorsal and plantar sections in the head and base. The raw dorsal and plantar BV/TV and DA values were also compared between species using Kruskal-Wallis tests to test whether the samples originate from the same distribution. Additionally, BV/TV values in both epiphyses were used to calculate the ratio of trabecular bone in the plantar versus dorsal regions. Ratios were compared between taxa using a pairwise Wilcoxon rank sum test with a Bonferroni correction. In addition to traditional non-parametric tests, differences between the BV/TV ratios of each taxon were evaluated for statistical significance using a standard resampling method (i.e., bootstrapping), which is well-suited to examine differences between means of groups with varying and small sample sizes (Efron and Tibshirani, 1993). Values from each taxon were resampled with replacement 10,000 times, from which 10,000 BV/TV ratio means were generated. Using pairwise comparison, the bootstrapped means from all taxa were randomly aligned and subtracted from means from another taxon, resulting in 10,000 differences between the means. Pairwise comparison was also used to calculate the difference between the means of the original, non-bootstrapped samples. The bootstrapped differences were then compared to the original differences. The number of times the difference between the bootstrapped means exceeded the difference between the original sample means represents a proportion that is analogous to a p-value of a one-tailed test.

Bootstrap analysis was also applied to the fossil sample to determine the likelihood that their BV/TV ratios fell within those of the extant taxa. In this case, the BV/TV ratio from the fossil was included within each extant taxon's sample, which was then resampled and replaced. The number of

times the fossil's BV/TV ratio fell within the range of the bootstrapped mean BV/TV ratios represents the likelihood that this value would be expected within a sample from the study taxa.

3. Results

3.1. Allometry

Most trabecular parameters showed no significant allometric scaling within taxa (**Table 2**). *Gorilla* showed positive scaling of trabecular thickness and a negative scaling of trabecular number. However, while this correlation was significant for trabecular thickness ($p<0.05$), the confidence intervals of the slope contained the isometric scaling value, meaning isometry cannot be rejected. The same pattern is seen in modern humans, though none of the scaling is significant. *Pan* shows significant positive and negative allometric scaling of trabecular spacing and number, respectively. *Pongo* shows positive scaling for trabecular thickness and negative scaling for trabecular spacing. However, it shows no significant allometric scaling. In all taxa, BV/TV and DA both show a positive relationship with increased MT1 size, but without any significant positive allometric scaling. *Pan* presents a single exception, wherein BV/TV has a negative relationship with MT1 size, though it is not statistically significant. This allows for the conclusion that BV/TV and DA are not strongly linked to MT1 size (and by proxy, body size). Given the fact that BV/TV does not scale allometrically in any taxon, it can be concluded that body size, and by extension sex do not affect patterns of trabecular distribution to a significant degree.

3.2. MT1 BV/TV distribution

Figure 3 shows BV/TV distribution maps of a representative specimen from each taxon within the sample (images of the full sample are shown within the supplementary information, Figs. 1 – 4). Modern humans consistently show a greater distribution of trabecular bone within the dorsal aspect of the head. However, some individuals have higher BV/TV values closer to the centre of the epiphysis or near the cortical/trabecular boundary. BV/TV tends to be higher on the lateral side of the dorsal aspect, corresponding with the slightly valgus orientation of the phalanges in relation to the metatarsal shaft. Additionally, specimens show a consistent pattern on the plantar surface of the head wherein the trabecular bone directly below the articular surface for the sesamoid bones displays lower

BV/TV (see SI, Fig. S4). The ventral keel between the articular surfaces has generally higher BV/TV. All modern humans have higher BV/TV on the dorsal half of the MT1 base; the plantar aspect has relatively little trabecular bone, with the exception of a small area near the insertion site of the fibularis longus tendon, which is more pronounced in modern humans than in non-human apes.

All non-human apes within the sample tend to exhibit a higher concentration of trabecular bone within the plantar region of the head, with *Pongo* showing the most plantar concentration. *Pan* and *Gorilla* show relatively similar distributions to each other; trabecular bone has a higher concentration on the plantar aspect of the head, but it is further from the subchondral boundary than in *Pongo*. However, in all taxa, there is variability in the extent to which the trabecular bone extends into the centre of the distal epiphysis: some individuals have a fairly localized concentration near the subchondral bone, but others show a much deeper distribution within the entire epiphysis (e.g., see SI Figs 1-3). The pattern of trabecular bone distribution within the base is variable, but overall it is evenly distributed across the dorsal and plantar regions. *Pongo* shows a pattern in which the edges of the articular surface show higher BV/TV (see Fig. 2), with relatively less trabecular bone in the center of the epiphysis. In all non-human apes, the trabecular bone is distributed along an oblique plane in relation to the shaft, corresponding to the plane in which the metatarsal flexes and extends.

Figures 4 and 5 illustrate the external morphology and trabecular distribution of SKX 5017 and SK 1813, respectively. Similar to modern humans, the dorsal region of the metatarsal head of SKX 5017 exhibits a higher distribution of trabecular bone than the plantar region; although it is located more dorsally than is generally found within modern humans. This region of high BV/TV is positioned laterally and corresponds to a slightly valgus orientation of the phalanges in relation to the shaft. The remainder of the head shows an even distribution of trabecular bone, with an area of slightly higher BV/TV on the plantar aspect on the ventral keel between the articular surfaces for the sesamoid bones (this is also seen in some modern humans). The base of SKX 5017 shows high BV/TV near the dorso-medial border of the articular surface, similar to where it is seen in several non-human apes, and a slight area of high BV/TV on the plantar-lateral aspect. Both plantar and dorsal regions display high BV/TV, in contrast to modern humans which have a markedly higher and more localized trabecular bone distribution within the dorsal region.

SK 1813 (**Fig. 5**) also displays higher trabecular bone distribution within the dorsal aspect of the head, though it is more centralized within the epiphysis than in SKX 5017 or the modern human sample. Additionally, the area immediately below the cortical/trabecular boundary shows a sharp decrease in BV/TV. On the plantar aspect, where the shaft meets the head, there is another area of high BV/TV. When comparing the color map to the original CT scan, it becomes apparent that this area of high BV/TV is the result of cortical bone from the shaft extending into thick trabecular struts within the head, similar to *Pan* and *Gorilla*. However, SK 1813 shows relatively less trabecular bone within the rest of the plantar surface, resulting in a different overall distribution to all other taxa.

3.3. Regional trabecular distribution

Mean values for all trabecular parameters are shown in **Table 3,** and **Figure 6** presents box-and-whisker plots of BV/TV values among the study taxa. Within extant taxa, BV/TV tends to be highest in *Pan* and lowest in modern humans. Furthermore, modern humans show the highest overall DA values, and *Pongo* displays the lowest. It should be noted that coefficients of variation (CV) indicate that *Pongo* has the most variable BV/TV and DA values (with the exception of BV/TV in the modern human base). When considering overall patterns across both epiphyses, trabecular thickness is highest in *Gorilla* and lowest in modern humans. Trabecular number shows the opposite pattern: it is highest in modern humans and lowest in *Gorilla*. Trabecular spacing is highest in *Gorilla*; of the extant sample, it is lowest in modern humans. When considering the base and head separately, different patterns emerge between taxa. Although BV/TV is similar between the head and base, all extant non-human apes show a relatively higher number, and more tightly spaced trabeculae in the base than in the head. In all cases, BV/TV remains similar in both epiphyses as a result of thinner trabecular bone in the base. We also see a difference in DA between the head and base: despite some overlap in values, mean DA is higher in the base than in the head. In contrast, modern humans show a similar trabecular architecture in the head and in the base. Trabecular number is slightly higher in the head, resulting in higher BV/TV, but to a lesser extent than the non-human apes.

The two fossils show a different trabecular bone structure from each other, as well as to the comparative sample. SKX 5017 exhibits the highest overall BV/TV of all taxa as a result of a

relatively higher number of thicker and closely spaced trabeculae. Similar to the non-human apes, it has a relatively higher number, and more closely spaced trabeculae in the base than in the head. SK 1813 shows a BV/TV value that falls well within the range of the African great apes. Its trabecular number is higher, and its trabecular spacing is lower than all other taxa. Its trabecular thickness falls within the range of all taxa. Both fossils have closely spaced trabeculae, but compared to SKX 5017, SK 1813 has a higher number of thinner trabeculae. Disregarding their absolutely thicker trabeculae than modern humans, the MT1 heads of the fossil specimens have an overall higher number of closely spaced trabeculae, a pattern seen in the head of modern humans; SKX 5017 shows values in the base within the range of non-human apes.

Regional summary statistics for all analyzed trabecular parameters can be seen in the SOM (SOM Table S1). Mann-Whitney U tests reveal significant differences in mean BV/TV values between the dorsal and plantar regions of the MT1 heads of all studied taxa (Fig. 6). Non-human apes show a higher BV/TV within the plantar region, whereas modern humans have higher BV/TV in the dorsal region. Within the base of the MT1, only modern humans show significant differences in BV/TV between the dorsal and plantar regions, with relatively higher values in the dorsal region. SKX 5017 shows higher BV/TV in the dorsal regions of the head and base, similar to modern humans, but with overall higher BV/TV. The SK 1813 head displays overall higher BV/TV in the dorsal region as well, though it has absolutely lower BV/TV than SKX 5017.

Figure 7 presents ratios of dorsal-to-plantar BV/TV within the heads and bases of all taxa. Within all non-human apes, the base of the metatarsal shows a BV/TV ratio approximating a value of one, indicating relatively equal BV/TV between the dorsal and plantar regions. In contrast, modern humans display a much higher ratio, indicating relatively higher BV/TV within the dorsal section of the base. Within the head, all extant non-human apes show a ratio below one, indicating relatively higher BV/TV within the plantar region, whereas modern humans retain a higher proportion of trabecular bone within the dorsal region. Results from post-hoc pairwise Wilcoxon rank sum tests from the head reveal significant differences between the BV/TV ratio of modern humans and all extant non-human apes ($p<0.0005$), and between *Gorilla* and *Pongo* ($p<0.01$) (**Table 4**). No statistically significant differences were found between *Pongo* and *Pan*, or between *Gorilla* and *Pan*.

Within the base, no statistically significant differences were found in BV/TV ratio between the non-human apes, but all showed significant differences from modern humans ($p<0.0005$). Bootstrap analyses support these results, showing a similar distribution of trabecular bone within the base of all non-human apes (see SI Fig. S6).

Results from bootstrap analyses of BV/TV ratio means in the base reveal significant differences between the BV/TV ratio of SKX 5017 and all extant taxa, with a value lower than modern humans ($p<0.01$), and higher than *Pongo* ($p<0.01$), *Gorilla* ($p<0.01$), and *Pan* ($p<0.01$) (**Fig. 8**). Bootstrap analyses from the head show that the BV/TV ratio of SKX 5017 falls within the range of modern humans ($p>0.05$), and that the BV/TV ratio of SK 1813 falls outside the range of all extant taxa ($p<0.01$). The distribution, though more dorsal than plantar, falls below the range seen in modern humans, and above the range seen *Pongo*, *Gorilla*, and *Pan* (**Fig. 9**).

Differences in DA values between taxa are illustrated in **Figure 10**. All taxa show significant differences between DA in the plantar and dorsal regions, with modern humans showing the absolute highest values, and *Pongo* the lowest. Results from the Kruskal-Wallis post hoc test for differences in DA show that modern humans have significantly higher DA in the head than all taxa, and significantly higher DA in the base than *Pongo* and *Gorilla*. Among the non-human apes, only *Pan* and *Pongo* differ significantly in the head. In the base, *Pan* is the only significantly different taxon, with the highest mean DA value (**Table 5**). There is no statistically significant interspecies difference in the ratio of DA between the dorsal and plantar regions. All modern taxa display a pattern where the dorsal sections of both epiphyses possess similar DA values that are significantly higher than the values seen in the plantar sections. Like the modern taxa, SKX 5017 displays higher DA in the dorsal regions, however, DA in the dorsal region of the base is absolutely higher than DA in the dorsal region of the head, and DA in the plantar region of the base is absolutely higher than the plantar region of the head. The plantar region of the base and the dorsal region of the head share close values, a pattern not seen in the entire extant sample. SK 1813 displays a similar DA pattern to the extant taxa, with higher values in the dorsal region than in the plantar region, although it has the absolute lowest values.

Figures 11 and **12** display bivariate plots of BV/TV and DA values from the head and base, respectively. Modern humans possess lower BV/TV and higher DA, distinguishing them from other taxa. Within the non-human apes, *Pan* shows overall higher DA, followed by *Gorilla* and *Pongo*, respectively, but their BV/TV values overlap. As mentioned earlier, *Pongo* shows the widest range of BV/TV values. BV/TV values in both SKX 5017 and SK1813 are well above those in modern humans, and within the range of the non-human apes**.** DA values are lower in SK 1813 and SKX 5017 than in modern humans, though they are absolutely lowest in the former, within the range of *Pongo*.

4. Discussion

4.1. Effect of body size on trabecular bone structure

Most trabecular parameters do not to scale allometrically within species. Like other studies (Doube et al., 2011; Ryan and Shaw, 2013), results from this analysis show a positive, but isometric relationship between BV/TV and body size. The only taxon to show positive scaling of trabecular thickness is *Gorilla*, supporting previous findings (Doube et al., 2011). However, because the confidence intervals of the slope contain the isometric scaling value, an isometric relationship cannot be rejected. All other taxa show no allometric scaling of trabecular thickness (see also Mullender et al., 1996; Swartz et al., 1998). In *Pan*, trabecular spacing shows positive allometric scaling and trabecular number shows negative allometric scaling. These results contradict previous studies of trabecular allometry in primates (mainly in the femur and humerus), which emphasize negative allometric scaling of trabecular spacing and thickness (Ryan and Ketcham, 2002, 2005; Fajardo et al., 2007; Ryan and Walker, 2010; Ryan and Shaw, 2012). This could be the result of smaller sample sizes used in this study, or because this study observes interspecies allometry. Our results are partially consistent with a previous study on allometry between *Pan* and *Homo* (Tsegai et al., 2017). Certain trabecular variables of the MT1 show similar scaling patterns as the talus, but others are more consistent with the distal tibia. Overall, these results suggest that scaling within species as a result of individual size variation and sexual dimorphism do not play an important role in trabecular structure, and that different elements throughout the skeleton may show variable allometric scaling patterns.

4.2. Trabecular distribution in extant taxa

554 Within the extant sample, the trabecular parameters that most effectively separate each
555 locomotor mode are relative BV/TV and absolute DA. Trabecular bone acts as structural support
556 during joint loading, meaning higher BV/TV should be located in the area of the epiphysis where the
557 joint incurs high compressive loading (Rubin et al., 2002; Barak et al., 2011). A higher distribution of
558 trabecular bone in the plantar region offers support for loading during plantarflexion, and a higher
559 distribution in the dorsal region offers support for loading during dorsiflexion. The first hypothesis is
560 that modern humans show higher BV/TV within the dorsal aspect of the epiphyses. This is supported
561 here based on significantly higher BV/TV ratio in the MT1 of modern humans than all other extant
562 taxa, which corresponds to its higher range of dorsal excursion, and to the position in which the MTP
563 joint incurs maximum loading (Rodgers, 1995; Donahue and Sharkey, 1999; Vereecke et al., 2003;
564 D'Août et al., 2004). Furthermore, the tarsometatarsal joint, which is more limited in mobility than
565 the MTP joint, is stable and experiences movement along a single plane (Morton, 1924; Susman and
566 Brain, 1988; Proctor et al. 2008; Gill et al. 2015). Therefore, it exhibits a tightly constrained pattern
567 within the base of the MT1.
568 Within the head, non-human apes show a plantar distribution of trabecular bone associated
569 with high compressive loading during plantarflexion. This corresponds to studies of plantar pressure
570 distribution in *Pan troglodytes* (Wunderlich and Ischinger, 2017), which show that the MTP joint
571 incurs peak plantar pressure during vertical climbing, when it is plantarflexed. Plantar pressure data
572 on *Pongo* during suspensory locomotion is entirely absent, making inferences about loading at its
573 MTP joint speculative. However, results from this study suggest that it was nonetheless loaded higher
574 in plantarflexion than dorsiflexion. Although the *Pongo* hallux is less capable of force gripping
575 compared to *Gorilla* and *Pan*, its actual use during suspensory locomotion may not be as limited as
576 previously thought. Commonly held ideas emphasize that *Pongo* show reduced hallucal recruitment
577 during suspensory locomotion (Morton, 1924; Midlo, 1934; Tuttle and Rogers, 1966; Tuttle, 1969;
578 Marchi, 2010), however, there is evidence that its true use is somewhat underreported (McClure et al.,
579 2012).
580 The great apes, which have a more mobile tarsometatarsal joint, show evenly distributed
581 BV/TV within the entire base. This could be reflective of the variable ways in which these taxa load

582 the forefoot, resulting in a generalized trabecular structure adapted for a wide range of motion and
583 loading. Despite similar BV/TV ratios, color maps show differences in the distribution of trabecular
584 bone within the base of *Pongo*, *Gorilla*, and *Pan.* As mentioned earlier, trabecular bone within the
585 *Pongo* base shows a higher distribution near the edges of the articular surface, whereas *Gorilla* and
586 *Pan* show a relatively higher distribution throughout the entire epiphysis. This could be related to
587 locomotor differences between the taxa. *Pongo* employs a hook-like grip during suspension without
588 applying significant force on its hallux, contrary to *Pan* and *Gorilla*, which both use the hallux more
589 forcefully (Sarmiento, 1994; Remis, 1995; Oishi et al., 2012). The low compressive and tensile forces
590 experienced by the *Pongo* MT1 base might explain why the trabecular bone does not extend as far
591 into the centre of the epiphysis. This could mean that BV/TV ratio is better at differentiating broad
592 locomotor patterns (i.e., between bipedalism and vertical climbing), whereas BV/TV color maps may
593 better capture subtle differences in joint positioning and loading between types of terrestrial
594 quadrupedalism or arboreal locomotion.

595 Griffin et al. (2010b) analyzed the trabecular structure within the MT1 head of *Pongo*,
596 *Gorilla*, *Pan*, and *Homo*. By placing three VOIs in the epiphyses, they found that all taxa showed
597 higher BV/TV in the dorsal region of the head. Based on these results, they concluded that BV/TV
598 was not useful in differentiating habitual joint positioning. Results from this study contradict these
599 results. Though BV/TV ratio is not useful in differentiating locomotion between non-human apes, it
600 separates bipedalism from all other forms of locomotion. The reason for these conflicting results
601 could be methodological. Although overall, non-human apes show higher BV/TV in the plantar region
602 of the head, there is variation in where within the epiphysis BV/TV is highest. Some specimens show
603 higher trabecular distribution near the subchondral bone, and others show higher distribution deeper
604 within the epiphysis (and our results indicate that concentrations are not always in the midline of the
605 joint). Thus, VOIs restricted to only a portion of the epiphysis capture only a subset of the variation
606 compared to a whole-epiphysis approach.

607 It is also worth noting that BV/TV ratio is likely better at differentiating between broad
608 locomotor modes because absolute BV/TV does not necessarily reflect the magnitude of load applied
609 to an element. Modern humans show systematically lower BV/TV than all other taxa, despite their

610 medial forefoot experiencing higher loading during push-off than non-human apes (Vereecke et al.,
611 2003). Lower overall BV/TV has been previously observed in other studies of cortical and trabecular
612 bone in modern humans (Lieberman, 1996; Chirchir et al., 2015; Saers et al., 2016; Tsegai et al.,
613 2017) and has been suggested to be linked to higher sedentism in relation to early hominins and recent
614 hunter-gatherers. Because the sample represented in this study is of likely shod and sedentary modern
615 humans, it is also worth noting that the low overall BV/TV values seen here may not reflect the entire
616 range of human variation (Shaw and Stock, 2009a, b; 2013; Ryan and Shaw, 2015; Saers et al., 2016).
617 For this reason, in this study, BV/TV is mainly relevant when its relative distribution is analyzed.
618 Further studies including shod and unshod populations, as well as hunter-gatherers may contribute to
619 our understanding of overall BV/TV within modern humans.

620 The second hypothesis is that modern humans show higher DA within the MT1 than all non-
621 human apes, and that this is most apparent in the dorsal regions. This is partially supported; modern
622 humans show overall higher DA than *Gorilla* and *Pongo* throughout both epiphyses, but they do not
623 differ significantly from *Pan* in the base. Nevertheless, higher overall DA within modern humans
624 corresponds with the hypothesis that a more uniaxial range of movement will result in stereotypically
625 oriented trabeculae. Similar to Griffin et al. (2010b), we found that all taxa show higher DA dorsally,
626 suggesting that non-biomechanic factors may influence this trabecular variable. As such, caution
627 should be applied when inferring locomotor behavior based on DA alone. Within non-human apes,
628 DA values overlap, meaning the modes of locomotion employed by these taxa cannot be as clearly
629 differentiated using DA. For example, given the fact that *Gorilla* is considered the most terrestrial
630 taxon, it is noteworthy that it is most similar in DA to *Pongo*, the most arboreal taxon. This may also
631 be explained by different factors; *Gorilla* may simply load its hallux in variable positions, or the
632 individuals in this sample may have been relatively arboreal. There is evidence that western lowland
633 gorillas display considerable arboreal behavior, with females spending more time on terminal
634 branches at frequencies similar to *Pan* (Remis, 1995, 1999). Because the gorillas in this study are all
635 western lowland, there is the possibility that they were also relatively arboreal. Ultimately, there may
636 be substantial overlap in degree of arboreality between non-human apes, making DA fairly weak in
637 differentiating their locomotor modes. These results simply demonstrate that modern humans have the

least variable MT1 positioning. In order to associate DA with a specific mode of locomotion, it may be more informative to look at directionality of trabeculae as opposed to overall DA or DA ratio. DA is a measure of how similarly aligned trabeculae are in relation to each other, but does not provide information on which axis the trabeculae are aligned in. Because trabeculae orient themselves along the principal axis of movement, the actual direction in which they are aligned might be more informative in reconstructing movement in a joint (Biewener et al., 1996; Ryan and Ketcham, 2002; Pontzer et al., 2006; Saparin et al., 2011). Future analyses could map, in the same manner as absolute values of trabecular variables, regional differences in primary trabecular orientation throughout the epiphysis.

Similarities in trabecular patterning between non-human apes are emphasized when plotting DA against BV/TV. The head shows considerable overlap in values; *Gorilla* overlaps with *Pongo* and *Pan* in both variables. Combined, modern humans do not show overlap in DA and BV/TV with the other taxa, but their values are close. This could be due to the fact that the range of motion at the MT1 head is limited to flexion and extension, meaning all taxa show a similar range of movement here. DA in the base distinguishes taxa better; this could be because the TMT joint may better reflect differences in hallucal positioning. The problem with this explanation is that modern humans and *Pan* show similar DA in base, despite known differences in joint loading and positioning at the TMT joint. Perhaps *Pan* loads this joint along a relatively constrained axis, although further observational and biomechanical analyses would have to be performed to test this. It is also worth noting that non-human apes show overall higher DA in the base than the head, whereas modern humans show similar values in both epiphyses. This could be reflective of the fact that the former load their proximal and distal MT1 joints in variable positions, contrary to relatively constrained modern human MT1.

Despite broad similarities in BV/TV and DA between non-human apes, differences can be observed between them when comparing other trabecular parameters (Tb.Th., Tb.Sp., Tb.N.). *Gorilla* displays relatively few, thick, and widely spaced trabeculae, whereas *Pongo* is characterized by relatively more, thinner, and closely spaced trabeculae. *Pan* shows values intermediate between *Pongo* and *Gorilla*. Of the non-human apes, the overall pattern in *Pongo* is most similar to modern humans, which have the thinnest trabeculae, but are similar in number and spacing. However, these

differences in trabecular properties among species may not be significantly different and small sample sizes may not reflect overall patterns within species; furthermore, the functional implication of these differences, if any, is unknown.

4.3. SKX 5017 and SK 1813

The original descriptions of SKX 5017 and SK 1813 (Susman and Brain, 1988; Susman and de Ruiter, 2004) suggest that both have a combination of primitive and derived features, and that based on multivariate analyses of various linear measurements, both were most similar to modern humans. Additional multivariate analysis has suggested a unique mode of locomotion in both specimens characterized by relatively facultative bipedalism (Zipfel and Kidd, 2006). Research on the proximal articular surface of both specimens has differentiated them from modern humans (Proctor et al., 2010) and from one another (Vernon, 2013). Proctor et al. (2010) measured the curvature of the surface using 3D geometric morphometric analysis, and found that SK 1813 did not group with modern humans but showed affinities to SKX 5017. Based on an 'ape-like' curvature, both were interpreted as belonging to *Paranthropus*. Another analysis groups SKX 5017 with *Pan* and western gorillas in terms of mediolateral articular surface curvature, and SK 1813 with modern humans and *Papio* (Vernon, 2013). Based on these conflicting results, it is difficult to determine how 'human-like' or 'ape-like' the proximal articular surface is, and even less so the locomotor behavior associated with this shape.

The third hypothesis is that the two fossils will show similar trabecular distribution to modern humans, but that the base of SKX 5017 will show lower DA than in modern humans due to its relatively concave proximal articular facet. This is partially supported: based on its BV/TV ratio, SKX 5017 shows a similar trabecular distribution to modern humans in the head, but its base displays a more even dorso-plantar trabecular distribution. As predicted, DA within the base of SKX 5017 is lower than in modern humans. Similar to modern humans and SKX 5017, the SK 1813 head shows a BV/TV ratio over one, indicating a dorsal distribution of trabecular bone. However, the ratio is significantly lower than in modern humans; in fact, it falls outside the range of all taxa within the comparative sample. Based on the color maps, SKX 5017 shows evidence of an MTP joint that was loaded in hyper-dorsiflexion. The external morphology of the head, specifically its raised superior

aspect in relation to the dorsum of the shaft, indicates it was capable of a wide range of dorsiflexion at the MTP joint (Susman and Brain, 1988). However, because of its dorsal mediolaterally narrow width, previous analyses have not reached a consensus on how the joint was loaded. It has been suggested that this combination of features prevented close-packing in dorsiflexion at the MTP joint, and resulted in instability during bipedal locomotion (Susman and Brain, 1988; Susman and de Ruiter, 2004). Though bootstrap analysis places SKX 5017 BV/TV ratio well within the range of modern humans, the color maps suggest the element was not loaded in the same way. SKX 5017 shows a hyper-dorsal distribution of bone not seen in modern humans. Because this is not seen in any of the comparative taxa, it cannot be linked with confidence to a specific type of locomotion. This may fit in with previous suggestions that the joint was less stable during dorsiflexion: because the joint did not close-pack in dorsiflexion it hyper-extended, resulting in a more dorsal trabecular distribution. When taking into account other trabecular parameters (i.e., DA), it could imply a form of locomotion not seen in modern taxa. For example, this concentration of trabecular bone could be caused by habitual hyper-dorsiflexion at the MTP joint from foot placement that is directly against a vertical substrate. This has been noted to occur in arboreal contexts in modern human populations that collect resources from trees and is directly associated with extreme dorsiflexion of the ankle and forefoot (Kraft et al., 2014). Research on midfoot flexibility in modern humans has also shown that lateral midfoot plantar pressure is strongly correlated to the magnitude of midfoot flexion, and that individuals with higher lateral midfoot plantar pressure tend to have increased dorsiflexion at the hallucal MTP joint (Bates et al., 2013; DeSilva and Gill, 2013; DeSilva et al., 2015). How the trabecular bone in the MT1 of such individuals is structured is not known. However, this suggests that hyper-dorsiflexion at the MTP joint of SKX 5017 could be the result of a fairly mobile midfoot lacking a human-like arch.

The trabecular structure of the base of the SKX 5017 MT1 combined with its external morphology emphasize a different loading pattern from modern humans. Susman and Brain (1988) described the hallux as adducted based on their description of the base as relatively flat and superoinferiorly orientated. However, geometric morphometric analyses have shown that it shares morphological affinities to *Gorilla*, including a relatively oblique curvature and a concave surface, albeit to a lesser extent (Proctor et al., 2008). Ultimately, because we don't have a complete *P.*

robustus foot, it is difficult to tell with certainty whether it was abducent or adducted. However, results here show that the base does not adhere to a completely modern human-like trabecular structure. Though SKX 5017 has a higher ratio of trabecular bone within the dorsal aspect, there is relatively more trabecular bone within the plantar region than is observed in modern humans. As a result, the BV/TV ratio within the base of SKX 5017 is lower than in modern humans, but higher than is observed in all other non-human apes. The higher BV/TV ratio in the head suggests the element was loaded in dorsiflexion. However, the relatively lower ratio in the base suggests it could have still been loaded in plantarflexion. Combined with the fact that the proximal articular surface is concave compared to modern humans, this could be reflective of a TMT joint that has retained adaptations for grasping. DA within the base also suggests the TMT joint was more mobile than in modern humans: it is within the range of *Gorilla*, *Pan*, and *Pongo*, and like these taxa, is higher within the base than the head. This implies that the two epiphyses were capable of differential movement, and that unlike in modern humans, the element was not tightly constrained at both joints.

Additional trabecular parameters emphasize the unique nature of its trabecular structure. Though its trabecular thickness is within the range of modern great apes, SKX 5017 shows a structure in the head characterized by a high number of closely spaced trabeculae, which is seen in the head of modern human MT1s. Trabecular parameters within the base fall within the range of modern non-human apes. The functional implication of this is not certain, but it emphasizes the unique trabecular structure of SKX 5017: it is more 'human-like' in the head, and more 'ape-like' in the base.

It is worth noting that there is a prominent osteophyte on the dorsal aspect of the shaft, proximal to the articular surface of the head. This could be the result of a traumatic injury sustained in life, or a condition called hallux rigidus, which produces exostoses on the head of the first metatarsal (Susman and Brain, 1988). However, this condition is accompanied with flexed interphalangeal joints, which conflicts with the distribution of trabecular bone in the metatarsal head that indicates a dorsiflexed rather than plantarflexed MTP joint.

Similar to modern humans and SKX 5017, SK 1813 shows a more dorsal trabecular distribution in the head, which is reflective of a joint that was habitually loaded in dorsiflexion. It has been described by Susman and de Ruiter (2004) as similar in morphology and function to SKX 5017;

both metatarsals have a short, strait shaft, and medio-laterally narrow dorsal aspect of the head. However, the trabecular structure reveals considerable differences between the two specimens. SK 1813 displays BV/TV that is absolutely lower than SKX 5017, within the range of *Pongo*, *Gorilla*, and *Pan*, and a lower DA, closer to the range of *Pongo.* The distribution of trabecular bone, though more dorsal than plantar, falls equally between the ranges of non-human apes and modern humans, meaning it does not conform to any modern pattern. It is difficult to interpret joint positioning of SK 1813 accurately because only the head was analyzed, and because it is a subadult. Though modern humans retain a relatively consistent locomotor mode throughout ontogeny (Sutherland et al., 1980; Beck et al., 1981; Raichlen et al., 2015: but see Zeininger et al., 2018), juvenile and subadult gorillas, chimpanzees, and bonobos display much more arboreal behavior than adults (Doran, 1997; Sarringhaus et al., 2014). Trabecular structure is known to change throughout ontogeny (Ryan and Krovitz, 2006; Gosman and Ketcham, 2009; Raichlen et al., 2015; Saers, 2017) especially in regards to DA (Gosman and Ketcham, 2009; Abel and Macho, 2011). Because its taxonomic affiliation and life history are uncertain, it is not known whether its locomotor repertoire was as variable throughout ontogeny as modern apes, or as constrained as modern humans. It is possible that this hominin would have loaded its hallux in variable positions based on its lower BV/TV ratio than modern humans, and that it experienced multiaxial loading based on its low DA.

Additionally, SK 1813 displays the absolute highest trabecular number and the lowest trabecular spacing, which is a pattern seen in modern humans and SKX 5017. The taxonomic affiliations of both specimens are currently uncertain; analyses of the external morphology have provided contradictory opinions (Susman and Brain, 1988; Susman and de Ruiter, 2004; Proctor et al., 2010; Vernon, 2013). Here, we have shown that the BV/TV ratios between the two fossils are considerably different, implying different types of MTP joint loading. However, all other trabecular parameters represent a normal range of variation when compared to the intraspecies variation in other living taxa. Based on these results, we can only suggest that these hominins incurred different joint loading during locomotion.

4.4. Interpretation of Paranthropus *locomotion*

Debates about australopith and *Paranthropus* locomotion have emphasized different types of locomotion based on conflicting morphological evidence that shows derived features adapted for bipedalism, and primitive features indicative of climbing and pedal grasping (Stern and Susman, 1983; Susman et al., 1984; Susman and Brain, 1988; Grine and Susman, 1991; Susman and de Ruiter, 2004). Research on *P. robustus* locomotion is fairly limited because postcranial fossils are scarce and often not securely attributed to the taxon. Its postcranial morphology is described as gracile and of small stature (McHenry, 1991), and its locomotion has been described as bipedal with a 'less efficient' gait compared to modern humans (Napier, 1964; Robinson, 1972). Additionally, its radial morphology has been suggested to indicate retained arboreal abilities (Grine and Susman, 1991). Recently, the locomotor behavior of . *boisei* has been characterized by combined terrestrial bipedalism and occasional arboreality based on scapular, radial, humeral, femoral, and tibial morphology (Dominguez-Rodrigo et al., 2013; Green et al., 2018). If *Paranthropus* represents a monophyletic group, it is possible that *P. robustus* would have had similar postcranial morphology to *P. boisei*. However, the efficacy of using postcranial elements in determining phylogenetic association is uncertain; additionally, despite potentially monophyletic status, postcranial morphology between the two species could vary based on differing ecological niches.

Recently, research on *P. robustus* pedal elements (TM 1517) has supported the idea of an overall bipedally adapted foot. Trabecular structure in the talus has been shown to display increased DA in parts of the element associated with a medial weight shift during the stance phase, and by extension a human-like bipedal gait (Su and Carlson, 2017). Nonetheless, interpretations are still uncertain: higher BV/TV in the lateral region was suggested to indicate a degree of lateral loading intermediate in magnitude between modern human and anthropoid tali. However, diaphyseal cross-sectional properties of an MT5 from Swartkrans (SKX 33380) suggest human-like loading in the lateral column of the foot (Dowdeswell et al., 2017). Although, as with other Swartkrans postcranial elements, it should be noted that this MT5 is not linked to *P. robustus* with absolute certainty. Cumulatively, analyses of *Paranthropus* locomotion based on trabecular structure and external morphology show features that suggest habitual bipedalism, with an indication that the overall structure of the foot was more mobile, allowing for multiaxial movement at the MTP and TMT joints

(Napier, 1964; Robinson, 1972; Susman and Brain, 1988; Susman and de Ruiter, 2004; Dominguez-Rodrigo et al., 2013; Dowdeswell et al., 2017; Su and Carlson, 2017).

Based on patterns of BV/TV and DA within the metatarsal, there is evidence that the *Paranthropus* foot (associated with SKX 5017) possessed a habitually dorsiflexing MTP joint that was capable of a relatively multiaxial range of movement. The taxonomic status of SKX 5017 is reasonably-well established, as the layer in which it was found (Member 1) is represented by more than 95% *Paranthropus* remains (Susman and Brain, 1988). We do not know exactly how its external morphology compares to early *Homo* MT1s, meaning we cannot rule out the possibility that this element belongs to early *Homo*. Susman and Brain (1988) have emphasized its morphological similarities with OH 8, and others have noted that the SKX 5017 base is more similar to *A. afarensis* (A.L. 333-54), suggesting it belongs to a different taxon than early *Homo* (Proctor, 2008; Vernon, 2013). However, either possibility is uncertain since we do not know the definite taxonomic status of OH 8 (DeSilva et al., 2010). Therefore, these interpretations can only be applied to *P. robustus* with reasonable certainty. It is not certain whether SK 1813 represents *P. robustus* as well, but the trabecular structure of the two fossil specimens is different in BV/TV ratio and DA, indicating different habitual joint loading. However, we refrain from making taxonomic attributions to SK 1813 based on trabecular structure alone. If the trabecular pattern preserved here represents its adult structure, it could indicate two different species (*P. robustus* and *Homo* sp.), but enough is not known about *Paranthropus* and early *Homo* postcranial variability to make that claim. Furthermore, if the trabecular structure seen in SK 1813 reflects a subadult mode of locomotion that differs from adult locomotion, it may very well represent the same species as SKX 5017 at an earlier ontogenetic stage.

5. Conclusions

Studies of trabecular bone structure have provided mixed results in its utility in inferring habitual joint positioning (Ryan and Ketcham, 2002; Fajardo et al., 2007; DeSilva and Devlin, 2012). However, it is possible that elements in closer contact to the substrate may be more reflective of locomotor behavior because they directly absorb compressive loads associated with ground reaction forces (Maga et al., 2006; Kivell, 2016). The MT1 shows particular promise because it is a relatively simple element with adjacent joints that show a consistent range of motion. Results from this study

strengthen its application in inferring fossil hominin locomotion by providing evidence that its trabecular structure can be linked to habitual joint positioning and loading of the forefoot within an extant ape sample. The most apparent differences are seen between modern humans and all other non-human apes, indicating that the relatively constrained and stable structure of the human foot results in specific trabecular patterning. BV/TV reflects the position in which the joint experiences the highest load, and DA reflects its range of motion. Though these parameters do not statistically differentiate variation in non-human ape locomotion, obligate bipedalism presents clear signals. Human bipedal locomotion is reflected in the dorsally distributed and anisotropic trabecular bone structure in the MT1, while the more arboreally adapted non-human MT1 exhibits more plantarly distributed, and relatively less anisotropic trabecular bone. This study also highlights the importance of trabecular bone analysis in the context of paleoanthropology. The two fossil specimens, which have been described as highly similar in external morphology, present different trabecular bone structures that would imply variable modes of locomotion. We find that the MTP joint was loaded differently in the two specimens: one in hyper-dorsiflexion, and the other in a manner intermediate between modern humans and non-human apes. Whether this is due to ontogenetic or phylogenetic factors is unknown. Ultimately, we show that trabecular bone structure can be associated with known modes of locomotion in modern taxa, and that it can be informative in in reconstructions of fossil hominin behavior.

Acknowledgements

For access to specimens, we thank the Max Planck Institute for Evolutionary Anthropology (Christoph Boesch and Jean-Jacques Hublin), the Powell-Cotton Museum (Inbal Livine), the Johann-Freidrich-Blumenbach-Institutfür Zoologie und Anthropologie der Georg-August-Universität Göttingen (Birgit Großkopf), and the Zoologische Staatsammlung Munich (Anneke van Heteren). For scanning, we thank David Plotzki (Max Plank Institute for Evolutionary Anthropology) and Keturah Smith (Cambridge University). For comments on previous versions of this manuscript we thank Leoni Georgiou.

Funding: This research was supported by the Max Planck Society (MMS) and the European Research Council Starting Grant #336301 (MMS) and the University of Kent (KK and MMS).

880 **References**

881 Abel, R., Macho, G.A., 2011. Ontogenetic changes in the internal and external morphology of the
882 ilium in modern humans. American Journal of Anatomy 218, 324-335.

883 Aerts, P., Van Damme, R., Van Elsacker, L., Duchêne, V., 2000. Spatio-temporal gait characteristics
884 of the hind-limb cycles during voluntary bipedal and quadrupedal walking in bonobos (*Pan*
885 *paniscus*). American Journal of Physical Anthropology 111, 503-517.

886 Barak, M.M., Lieberman, D.E., Hublin, J.-J., 2011. A Wolff in sheep's clothing: Trabecular bone
887 adaptation in response to changes in joint loading orientation. Bone 49, 1141-1151.
888 Barak, M.M., Lieberman, D.E., Hublin, J.-J., 2013. Of mice, rats and men: Trabecular bone
889 architecture in mammals scales to body mass with negative allometry. Journal of Structural
890 Biology 183, 123-131.
891 Bates, K.T., Collins, D., Savage, R., McClymont, J., Webster, E., Pataky, T.C., D'Août, K., Sellers,
892 W.I., Bennett, M.R., Crompton, R.H., 2013. The evolution of compliance in the human lateral
893 mid-foot. Proceedings of the Royal Society B 280, 20131818.
894 Beck, R.J., Andriacchi, T.P., Kuo, K.N., Fermier, R.W., Galante, J.O., 1981. Changes in the gait
895 patterns of growing children. Journal of Bone Joint Surgery 63, 1452-1457.
896 Berillon, G., 1999. Geometric pattern of the hominoid hallucal tarsometatarsal complex. Quantifying
897 the degree of hallux abduction in early hominids. Comptes Rendus de l'Académie des Sciences
898 IIA 328, 627-633.
899 Berger, L.R. and Hawks, J., 2019. *Australopithecus prometheus* is a nomen nudum. American Journal
900 of Physical Anthropology 168, 383-387.
901 Bertram, J., Swartz, S., 1991. The law of bone transformation - A case of crying Wolff. Biological
902 reviews of the Cambridge Philosophical Society 66, 245-273.
903 Biewener, A., Fazzalari, N., Konieczynski, D., Baudinette, R., 1996. Adaptive changes in trabecular
904 architecture in relation to functional strain patterns and disuse. Bone 19, 1-8.
905 Bøjsen-Moller, F., 1979. Calcaneocuboid joint and stability of the longitudinal arch of the foot at high
906 and low gear push off. Journal of Anatomy 129, 165-176.

907 Cant, J.G.H., 1987. Positional behavior of female bornean orangutans (*Pongo pygmaeus*). American
908 Journal of Primatology 12, 71-90.
909 Caravaggi, P., Pataky, T., Günther, M., Savage, R., Crompton, R., 2010. Dynamics of longitudinal
910 arch support in relation to walking speed: Contribution of the plantar aponeurosis. Journal of
911 Anatomy 217, 254-261.
912 Carlson, K.J. 2005. Investigating the form-function interface in African apes: Relationships between
913 principal moments of area and positional behaviors in femoral and humeral diaphyses. American
914 Journal of Physical Anthropology 127, 312-334.
915 Carlson, K.J., Lublinsky, S., Judex, S., 2008. Do different locomotor modes during growth modulate
916 trabecular architecture in the murine hind limb? Integrative and Comparative Biology 48, 385-
917 393.
918 Chang, G., Pakin, S.K., Schweitzer, M.E., Saha, P.K., Regatte, R.R., 2008. Adaptations in trabecular
919 bone microarchitecture in Olympic athletes determined by 7T MRI. Journal of Magnetic
920 Resonance Imaging: An Official Journal of the International Society for Magnetic Resonance in
921 Medicine 27, 1089-1095.
922 Chirchir, H., 2016. Limited trabecular bone density heterogeneity in the human skeleton. Anatomy
923 Research International 2016, 7.
924 Chirchir, H., Kivell, T.L., Ruff, C.B., Hublin, J.-J., Carlson, K.J., Zipfel, B., Richmond, B.G., 2015.
925 Recent origin of low trabecular bone density in modern humans. Proceedings of the National
926 Academy of Science 112, 366-371.
927 Christensen, J.C., Jennings, M.M., 2009. Normal and abnormal function of the first ray. Clinics in
928 Podiatric Medicine and Surgery 26, 355-371.
929 Clarke, R.J., Tobias, P.V., 1995. Sterkfontein Member 2 foot bones of the oldest South African
930 hominid. Science 269, 521-524.
931 Clarke, R.J., 2013. *Australopithecus* from Sterkfontein Caves, South Africa. In: Reed, K.E., Fleagle,
932 J.G., Leakey, R.E. (Eds.), The Paleobiology of *Australopithecus*. Springer, New York, pp. 105-
933 124.

934 Congdon, K. 2012. Interspecific and ontogenetic variation in proximal pedal phalangeal curvature of
935 great apes (*Gorilla gorilla*, *Pan troglodytes*, and *Pongo pygmaeus*). International Journal of
936 Primatology 33, 418-427.
937 Cowin, S., Hart, R., Balser, J., Kohn, D., 1985. Functional adaptation in long bones - establishing *in*
938 *vivo* values for surface remodeling rate coefficients. Journal of Biomechanics 18, 665-&.
939 D'Août, K., Vereecke, E., Schoonaert, K., De Clercq, D., Van Elsacker, L., Aerts, P., 2004.
940 Locomotion in bonobos (*Pan paniscus*): Differences and similarities between bipedal and
941 quadrupedal terrestrial walking, and a comparison with other locomotor modes. Journal of
942 Anatomy 204 353-361.
943 Day, M.H., Napier, J.R. 1965. Fossil foot bones. Current Anthropology 6, 419-420.
944 De Groote, I., Humphrey, L.T., 2011. Body mass and stature estimation based on the first metatarsal
945 in humans. American Journal of Physical Anthropology 144, 625-632.
946 Delaunay, B., 1934. Sur la sphère vide. À la mémoire de Georges Voronoï. Izvestiya Akademiya
947 Nauk SSR, Seriya Geologicheskaya 793-800.
948 DeSilva, J.M., Zipfel, B., Van Arsdale, A.P., Tocheri, M.W., 2010. The Olduvai Hominid 8 foot:
949 adult or subadult? Journal of Human Evolution 5, 418-423.
950 DeSilva, J.M., Devlin, M.J., 2012. A comparative study of the trabecular bony architecture of the
951 talus in humans, non-human primates, and *Australopithecus*. Journal of Human Evolution 63,
952 536-551.
953 DeSilva, J.M., Gill, S.V., 2013. Brief communication: a midtarsal (midfoot) break in the human foot.
954 American Journal of Physical Anthropology 151, 495-499.
955 DeSilva, J.M., Holt, K.G., Churchill, S.E., Carlson, K.J., Walker, C.S., Zipfel, B., et al., 2013. The
956 lower limb and mechanics of walking in *Australopithecus sediba*. Science 340, 1232999.
957 DeSilva, J.M., Bonne-Annee, R., Swanson, Z., Gill, C.M., Sobel, M., Uy. J., Gill, S.V., 2015.
958 Midtarsal break variation in modern humans: functional causes, skeletal correlates, and
959 paleontological implications. American Journal of Physical Anthropology 156, 543-552.
960 DeSilva, J., McNutt, E., Benoit, J. and Zipfel, B., 2019. One small step: A review of Plio-Pleistocene
961 hominin foot evolution. American Journal of Physical Anthropology 168, 63-140.

962 Devlin, M.J., 2011. Estrogen, exercise, and the skeleton. Evolutionary Anthropology 20, 54-61.
963 Devlin, M.J., Bouxsein, M.L., 2012. Influence of pre- and peri-natal nutrition on skeletal acquisition
964 and maintenance. Bone 50, 444-451.
965 Devlin, M.J., Grasemann, C., Cloutier, A.M., Louis, L., Alm, C., Palmert, M.R., Bouxsein, M.L.,
966 2013. Maternal perinatal diet induces developmental programming of bone architecture. Journal
967 of Endocrinology 217, 69-81.
968 Doden, E., 1993. The relationship between the function and the inner cortical structure of metacarpal
969 and phalangeal bones. In: Preuschoft, H., Chivers, D. J. (Eds.), Hands of Primates. Springer,
970 Vienna, pp. 271-284.
971 Domínguez-Rodrigo, M., Pickering, T.R., Baquedano, E., Mabulla, A., Mark, D.F., Musiba, C., Bunn,
972 H.T., Uribelarrea, D., Smith, V., Diez-Martin, F. Pérez-González, A., 2013. First partial skeleton
973 of a 1.34-million-year-old *Paranthropus boisei* from Bed II, Olduvai Gorge, Tanzania. PLoS
974 One 8, e80347.
975 Donahue, S.W., Sharkey, N.A. 1999. Strains in the metatarsals during the stance phase of gait:
976 Implications for stress fractures. Journal of Bone Joint Surgery 81, 1236-1244.
977 Doran, D.M. 1993a. Comparative locomotor behavior of chimpanzees and bonobos - the influence of
978 morphology on locomotion. American Journal of Physical Anthropology 91, 83-98.
979 Doran, D.M., 1997. Ontogeny of locomotion in mountain gorillas and chimpanzees. Journal of
980 Human Evolution 32, 323-344.
981 Doube, M., Klosowski, M.M., Wiktorowicz-Conroy, A.M., Hutchinson, J.R., Shefelbine, S.J., 2011.
982 Trabecular bone scales allometrically in mammals and birds. Proceedings of the Royal Society B
983 - Biological Sciences 278, 3067-3073.
984 Dowdeswell, M.R., Jashashvili, T., Patel, B.A., Lebrun, R., Susman, R.L., Lordkipanidze, D.,
985 Carlson, K.J., 2017. Adaptation to bipedal gait and fifth metatarsal structural properties in
986 *Australopithecus*, *Paranthropus*, and *Homo*. Comptes Rendus Palevol 16, 585-599.
987 Drapeau, M.S.M., Harmon, E.H., 2013. Metatarsal torsion in monkeys, apes, humans and
988 *Australopiths*. Journal of Human Evolution 64, 93-108.

989 Dunmore, C.J., Wollny, G. Skinner, M.M., 2018. MIA-Clustering: a novel method for segmentation
990 of paleontological material. PeerJ 6, e4374.
991 Efron, B., Tibshirani, R., 1993. An introduction to the bootstrap. CRC Press, LLC, Boca Raton,
992 Florida.
993 Elftman, H., Manter, J., 1935. The evolution of the human foot, with especial reference to the joints.
994 Journal of Anatomy 70, 56-67.
995 Eriksen, E.F., 2010. Cellular mechanisms of bone remodeling. Reviews in Endocrine and Metabolic
996 Disorders 11, 219-227.
997 Fajardo, R.J., Muller, R., Ketcham, R.A., Colbert, M., 2007. Nonhuman anthropoid primate femoral
998 neck trabecular architecture and its relationship to locomotor mode. Anatomical Record 290,
999 422-436.
1000 Ferguson, W.W., 1989. A new species of the genus *Australopithecus* (primates: Hominidae) from
1001 Plio/Pleistocene deposits west of Lake Turkana in Kenya. Primates 30, 223-232.
1002 Fernández, P.J., Almécija, S., Patel, B.A., Orr, C.M., Tocheri, M.W., Jungers, W.L., 2015. Functional
1003 aspects of metatarsal head shape in humans, apes, and old world monkeys. Journal of Human
1004 Evolution 86, 136-146.
1005 Fox, J.C., Keaveny, T.M. 2001. Trabecular eccentricity and bone adaptation. Journal of Theoretical
1006 Biology 212, 211-221.
1007 Gebo, D.L., 1996. Climbing, brachiation, and terrestrial quadrupedalism: Historical precursors of
1008 hominid bipedalism. American Journal of Physical Anthropology 101, 55-92.
1009 Gebo, D.L., Schwartz, G.T. 2006. Foot bones from Omo: implications for hominid
1010 evolution. American Journal of Physical Anthropology 129, 499-511.
1011 Gill, C.M., Bredella, M.A., DeSilva, J.M., 2015. Skeletal development of hallucal tarsometatarsal
1012 joint curvature and angulation in extant apes and modern humans. Journal of Human Evolution
1013 88, 137-145.
1014 Gosman, J.H., Ketcham, R.A., 2009. Patterns in ontogeny of human trabecular bone from SunWatch
1015 village in the prehistoric Ohio valley: General features of microarchitectural change. American
1016 Journal of Physical Anthropology 138, 318-332.

1017 Green, D.J., Chirchir, H., Mbua, E., Harris, J.W., Braun, D.R., Griffin, N.L., Richmond, B.G., 2018.
1018 Scapular anatomy of *Paranthropus boisei* from Ileret, Kenya. Journal of Human Evolution 125,
1019 181-192.
1020 Griffin, N.L., D'Août, K., Richmond, B., Gordon, A., Aerts, P., 2010a. Comparative *in vivo* forefoot
1021 kinematics of *Homo sapiens* and *Pan paniscus*. Journal of Human Evolution 59, 608-619.
1022 Griffin, N.L., D'Août, K., Ryan, T.M., Richmond, B.G., Ketcham, R.A., Postnov, A., 2010b.
1023 Comparative forefoot trabecular bone architecture in extant hominids. Journal of Human
1024 Evolution 59, 202-213.
1025 Griffin, N.L., Richmond, B.G., 2005. Cross-sectional geometry of the human forefoot. Bone 37, 253-
1026 260.
1027 Griffin, N.L., Richmond, B.G., 2010. Joint orientation and function in great ape and human proximal
1028 pedal phalanges. American Journal of Physical Anthropology 141, 116-123.
1029 Griffin, N.L., Miller, C.E., Schmitt, D., D'Août, K., 2015. Understanding the evolution of the
1030 windlass mechanism of the human foot from comparative anatomy: Insights, obstacles, and
1031 future directions. American Journal of Physical Anthropology 156, 1-10.
1032 Grine, F.E., Susman, R.L. 1991. Radius of *Paranthropus robustus* from Member 1, Swartkrans
1033 formation, South Africa. American Journal of Physical Anthropology 84, 229-248.
1034 Grine, F.E. 1993. Description and preliminary analysis of new hominid craniodental fossils from the
1035 Swartkrans formation. Swartkrans: A Cave's Chronicle of Early Man.Transvaal Museum,
1036 Pretoria 75-116.
1037 Grine, F.E., Daegling, D.J. 1993. New mandible of *Paranthropus robustus* from member 1,
1038 Swartkrans formation, South Africa. Journal of Human Evolution 24, 319-333.
1039 Gross, T., Kivell T.L., Skinner, M.M., Nguyen, H., Pahr, D.H. 2014. A CT-image-based method for
1040 the holistic analysis of cortical and trabecular bone. Paleontologia Electronica 17, A17333.
1041 Guldberg, R.E., Richards, M., Caldwell, N.J., Kuelske, C.L., Goldstein, S.A., 1997. Trabecular bone
1042 adaptation to variations in porous-coated implant topology. Journal of Biomechanics 30, 147-
1043 153.

1044 Haile-Selassie, Y., Saylor, B.Z., Deino, A., Levin, N.E., Alene, M., Latimer, B.M., 2012. A new
1045 hominin foot from Ethiopia shows multiple Pliocene bipedal adaptations. Nature 483, 565-579.
1046 Harcourt-Smith, W.E.H., O'Higgins, P., Aiello, L.C., 2002. From Lucy to Littlefoot: a three
1047 dimensional analysis of Plio-Pleistocene hominin tarsal remains. American Journal of Physical
1048 Anthropology S34, 82-82.
1049 Harcourt-Smith, W.E.H., Aiello, L.C., 2004. Fossils, feet and the evolution of human bipedal
1050 locomotion. Journal of Anatomy 204, 403-416.
1051 Harcourt-Smith, W.E.H., Throckmorton, Z., Congdon, K.A., Zipfel, B., Deane, A.S., Drapeau,
1052 M.S.M., Churchill, S.E., Berger, L.R., DeSilva, J.M., 2015. The foot of *Homo naledi*. Nature
1053 Communications 6, 8432.
1054 Harrison, L.C., Nikander, R., Sikiö, M., Luukkaala, T., Helminen, M.T., Ryymin, P., Soimakallio, S.,
1055 Eskola, H.J., Dastidar, P., Sievänen, H., 2011. MRI texture analysis of femoral neck: Detection
1056 of exercise load-associated differences in trabecular bone. Journal of Magnetic Resonance
1057 Imaging 34, 1359-1366.
1058 Havill, L.M., Allen, M.R., Bredbenner, T.L., Burr, D.B., Nicolella, D.P., Turner, C.H., Warren, D.M.,
1059 Mahaney, M.C., 2010. Heritability of lumbar trabecular bone mechanical properties in baboons.
1060 Bone 46, 835-840.
1061 Hetherington, V.J., Carnett, J., Patterson, B.A. 1989. Motion of the first metatarsophalangeal joint.
1062 The Journal of Foot Surgery 28, 13-19.
1063 Hicks, J.H., 1954. The mechanics of the foot: II. The plantar aponeurosis and the arch. Journal of
1064 Anatomy 88, 25-30.1.
1065 Hodgskinson, R., Currey, J.D., 1990. Effects of structural variation on Young's modulus of non-
1066 human cancellous bone. Proceedings of the Institution of Mechanical Engineers Part H Journal
1067 of Engineering in Medicine 204, 43-52.
1068 Huiskes, R., Ruimerman, R., van Lenthe, G., Janssen, J. 2000. Effects of mechanical forces on
1069 maintenance and adaptation of form in trabecular bone. Nature 405, 704-706.
1070 Hunt, A.E., Smith, R.M., Torode, M., Keenan, A.M., 2001. Inter-segment foot motion and ground
1071 reaction forces over the stance phase of walking. Clinical Biomechanics 16, 592-600.

1072 Hutton, W.C., Dhanendran, M., 1981. The mechanics of normal and hallux valgus feet – a
1073 quantitative study. Clinical Orthopaedics and Related Research 157, 7-13.
1074 Inouye, S.E. 1992. Ontogeny and allometry of African ape manual rays. Journal of Human
1075 Evolution 23, 107-138.
1076 Jacobs, C.R., 2000. The mechanobiology of cancellous bone structural adaptation. Journal of
1077 Rehabilitation Research and Development 37, 209-216.
1078 Jashashvili, T., Dowdeswell, M.R., Lebrun, R., Carlson, K.J., 2015. Cortical structure of hallucal
1079 metatarsals and locomotor adaptations in hominoids. Plos One 10, e0117905.
1080 Judex, S., Garman, R., Squire, M., Donahue, L.R., Rubin, C., 2004. Genetically based influences on
1081 the site-specific regulation of trabecular and cortical bone morphology. Journal of Bone and
1082 Mineral Research 19, 600-606.
1083 Katoh, Y., Chao, E.Y., Laughman, R.K., Schneider, E., Morrey, B.F. (1983). Biomechanical analysis
1084 of foot function during gait and clinical applications. Clinical Orthopaedics and Related
1085 Research 177, 23-33.
1086 Kidd, R.S., O'Higgins, P., Oxnard, C.E., 1996. The OH8 foot: a reappraisal of the functional
1087 morphology of the hindfoot utilizing a multivariate analysis. Journal of Human Evolution 31,
1088 269-291.
1089 Kivell, T.L., 2016. A review of trabecular bone functional adaptation: What have we learned from
1090 trabecular analyses in extant hominoids and what can we apply to fossils? Journal of Anatomy
1091 228, 569-594.
1092 Kraft, T.S., Venkataraman, V.V., Dominy, N.J. 2014. A natural history of human tree
1093 climbing. Journal of Human Evolution 71, 105-118.
1094 Lambers, F.M., Koch, K., Kuhn, G., Ruffoni, D., Weigt, C., Schulte, F.A., Müller, R., 2013.
1095 Trabecular bone adapts to long-term cyclic loading by increasing stiffness and normalization of
1096 dynamic morphometric rates. Bone 55, 325-334.
1097 Lanyon, L.E., 1973. Analysis of surface bone strain in the calcaneus of sheep during normal
1098 locomotion: strain analysis of the calcaneus. Journal of Biomechanics 6, 41-42.

1099 Lanyon, L.E., 1974. Experimental support for the trajectorial theory of bone structure. Journal of
1100 Bone and Joint Surgery 56, 160-166.
1101 Latimer, B.M., Lovejoy, C.O., Johanson, D.C., Coppens, Y. 1982. Hominid tarsal, metatarsal, and
1102 phalangeal bones recovered from the Hadar formation: 1974–1977 collections. American Journal
1103 of Physical Anthropology 57, 701-719.
1104 Latimer, B.M., Lovejoy, C.O., 1990. Hallucal tarsometatarsal joint in *Australopithecus afarensis*.
1105 American Journal of Physical Anthropology 82, 125-133.
1106 Lazenby, R.A., Skinner, M.M., Kivell, T.L., Hublin, J.-J., 2011. Scaling VOI size in 3D µCT studies
1107 of trabecular bone: A test of the over-sampling hypothesis. American Journal of Physical
1108 Anthropology 144, 196-203.
1109 Leakey, L.S., Tobias, P.V., Napier, J.R., 1964. A new species of the genus *Homo* from Olduvai
1110 Gorge. Nature 202, 7-9.
1111 Lee, C.R., Farley, C.T., 1998. Determinants of the center of mass trajectory in human walking and
1112 running. Journal of Experimental Biology 201, 2935-2944.
1113 Legendre, P., 2018. lmodel2: Model II Regression. R package version 1.7-3.
1114 Lieberman, D., 1996. How and why humans grow thin skulls: Experimental evidence for systemic
1115 cortical robusticity. American Journal of Physical Anthropology 101, 217-236.
1116 Lisowski, F.P. 1967. Angular growth changes and comparisons in the primate talus. Folia
1117 Primatologica 7, 81-97.
1118 Lorenzo, C., Arsuaga, J.L., Carretero, J.M. 1999. Hand and foot remains from the Gran Dolina Early
1119 Pleistocene site (Sierra de Atapuerca, Spain). Journal of Human Evolution 37, 501-522.
1120 Lovejoy, C.O. 2009. Reexamining human origins in light of *Ardipithecus ramidus*. Science 326, 74-
1121 74e8.
1122 MacLatchy, L., Muller, R., 2002. A comparison of the femoral head and neck trabecular architecture
1123 of *Galago* and *Perodicticus* using micro-computed tomography (µCT). Journal of Human
1124 Evolution 43, 89-105.

1125 Maga, M., Kappelman, J., Ryan, T., Ketcham, R., 2006. Preliminary observations on the calcaneal
1126 trabecular microarchitecture of extant large-bodied hominoids. American Journal of Physical
1127 Anthropology 129, 410-417.
1128 Maquer, G., Musy, S.N., Wandel, J., Gross, T., Zysset, P.K., 2015. Bone volume fraction and fabric
1129 anisotropy are better determinants of trabecular bone stiffness than other morphological
1130 variables. Journal of Bone Mineral Research 30, 1000-1008.
1131 Marchi, D., 2005. The cross-sectional geometry of the hand and foot bones of the Hominoidea and its
1132 relationship to locomotor behavior. Journal of Human Evolution 49, 743-761.
1133 Marchi, D., 2010. Articular to diaphyseal proportions of human and great ape metatarsals. American
1134 Journal of Physical Anthropology 143, 198-207.
1135 McClure, N.K., Phillips, A.C., Vogel, E.R., Tocheri, M.W., 2012. Unexpected pollex and hallux use
1136 in wild *Pongo pygmaeus wurmbii*. American Journal of Physical Anthropology 54(S), 208.
1137 McHenry, H.M., 1991. Petite bodies of the robust australopithecines. American Journal of Physical
1138 Anthropology 86, 445-454.
1139 McHenry, H.M., Coffing, K. 2000. *Australopithecus* to *Homo*: transformations in body and
1140 mind. Annual Review of Anthropology 29, 125-146.
1141 McHenry, H.M., Jones, A.L., 2006. Hallucial convergence in early hominids. Journal of Human
1142 Evolution 50, 534-539.
1143 Midlo, C., 1934. Form of hand and foot in primates. American Journal of Physical Anthropology 19,
1144 337-389.
1145 Mittra, E., Rubin, C., Qin, Y., 2005. Interrelationship of trabecular mechanical and microstructural
1146 properties in sheep trabecular bone. Journal of Biomechanics 38, 1229-1237.
1147 Morton, D.J., 1922. Evolution of the human foot. American Journal of Physical Anthropology 5, 305-
1148 336.
1149 Morton, D.J., 1924. Evolution of the human foot II. American Journal of Physical Anthropology 7, 1-
1150 52.

1151 Mullender, M.G., Huiskes, R., Versleyen, H., Buma, P. 1996. Osteocyte density and
1152 histomorphometric parameters in cancellous bone of the proximal femur in five mammalian
1153 species. Journal of Orthopaedic Research 14, 972-979.
1154 Munro, C.F., Miller, D.I., Fuglevand, A.J., 1987. Ground reaction forces in running: a
1155 reexamination. Journal of Biomechanics 20, 147-155.
1156 Napier, J.R., 1964. The evolution of bipedal walking in the hominids. Archives of Biological Sciences
1157 37, 3.
1158 Nester, C., Jones, R.K., Liu, A., Howard, D., Lundberg, A., Arndt, A., Stacoff, A. Wolf, P., 2007.
1159 Foot kinematics during walking measured using bone and surface mounted markers. Journal of
1160 Biomechanics 40, 3412.
1161 Odgaard, A., 1997. Three-dimensional methods for quantification of cancellous bone architecture.
1162 Bone 20, 315-328.
1163 Oishi, M., Ogihara, N., Endo, H., Une, Y., Ichihara, N., Asari, M., Amasaki, H., 2012. Muscle
1164 dimensions of the foot in the orangutan and the chimpanzee. Journal of Anatomy 221, 311-317.
1165 Pahr, D.H., Zysset, P.K., 2009. From high-resolution CT data to finite element models: Development
1166 of an integrated modular framework. Computer Methods in Biomechanics and Biomedical
1167 Engineering 12, 45-57.
1168 Pickering, R., Kramers, J.D., 2010. Re-appraisal of the stratigraphy and determination of new U-Pb
1169 dates for the Sterkfontein hominin site, South Africa. Journal of Human Evolution 59, 70-86.
1170 Polk, J.D., Blumenfeld, J., Ahluwalia, D., 2008. Knee posture predicted from subchondral apparent
1171 density in the distal femur: an experimental validation. The Anatomical Record: Advances in
1172 Integrative Anatomy and Evolutionary Biology 291, 293-302.
1173 Pontzer, H., Lieberman, D., Momin, E., Devlin, M., Polk, J., Hallgrimsson, B., Cooper, D.M.L., 2006.
1174 Trabecular bone in the bird knee responds with high sensitivity to changes in load orientation.
1175 Journal of Experimental Biology 209, 57-65.
1176 Pontzer, H., Rolian, C., Rightmire, G.P., Jashashvili, T., Ponce de León, M.S., Lordkipanidze, D.,
1177 Zollikofer, C.P., 2010. Locomotor anatomy and biomechanics of the Dmanisi hominins. Journal
1178 of Human Evolution 58, 492-504.

1179 Proctor, D.J., 2010. Brief communication: Shape analysis of the MT 1 proximal articular surface in
1180 fossil hominins and shod and unshod *Homo*. American Journal of Physical Anthropology 143,
1181 631-637.
1182 Proctor, D.J., Broadfield, D., Proctor, K., 2008. Quantitative three-dimensional shape analysis of the
1183 proximal hallucial metatarsal articular surface in *Homo, Pan, Gorilla*, and *Hylobates*. American
1184 Journal of Physical Anthropology 135, 216-224.
1185 Raichlen, D.A., Gordon, A.D., Foster, A.D., Webber, J.T., Sukhdeo, S.M., Scott, R.S., Gosman, J.H.,
1186 Ryan, T.M., 2015. An ontogenetic framework linking locomotion and trabecular bone
1187 architecture with applications for reconstructing hominin life history. Journal of Human
1188 Evolution 81, 1-12.
1189 Rafferty, K.L. and Ruff, C.B., 1994. Articular structure and function in *Hylobates*, *Colobus*, and
1190 *Papio*. American Journal of Physical Anthropology 94, 395-408.
1191 Räth, C., Baum, T., Monetti, R., Sidorenko, I., Wolf, P., Eckstein, F., Matsuura, M., Lochmüller,
1192 E.M., Zysset, P.K., Rummeny, E.J. and Link, T.M., 2013. Scaling relations between trabecular
1193 bone volume fraction and microstructure at different skeletal sites. Bone 57, 377-383.
1194 Remis, M.J., 1995. Effects of body size and social context on the arboreal activities of lowland
1195 gorillas in the Central African Republic. American Journal of Physical Anthropology 97, 413-
1196 433.
1197 Remis, M.J., 1999. Tree structure and sex differences in arboreality among western lowland gorillas
1198 (*Gorilla gorilla gorilla*) at Bai Hokou, Central African Republic. Primates 40, 383-396.
1199 Richmond, B.G. 2007. Biomechanics of phalangeal curvature. Journal of Human Evolution 53, 678-
1200 690.
1201 Robinson, J.T. 1972. Early hominid posture and locomotion. University of Chicago Press.
1202 Rodgers, M.M. 1995. Dynamic foot biomechanics. Journal of Orthopaedic and Sports Physical
1203 Therapy 21, 306-316.
1204 RStudio Team (2015). RStudio: Integrated Development for R. RStudio, Inc., Boston.

1205 Rubin, C., Turner, A.S., Mallinckrodt, C., Jerome, C., Mcleod, K., Bain, S., 2002. Mechanical strain,
1206 induced noninvasively in the high-frequency domain, is anabolic to cancellous bone, but not
1207 cortical bone. Bone 30, 445-452.
1208 Ruff, C., 1983. The contribution of cancellous bone to long-bone strength and rigidity. American
1209 Journal of Physical Anthropology 61, 141-143.
1210 Ruff, C., Runestad, J., 1992. Primate limb bone structural adaptations. Annual Review of
1211 Anthropology 21, 407-433.
1212 Ruff, C., Holt, B., Trinkaus, E., 2006. Who's afraid of the big bad Wolff? Wolff's Law and bone
1213 functional adaptation. American Journal of Physical Anthropology 129, 484-498.
1214 Ryan, T.M., Ketcham, R.A., 2002. The three-dimensional structure of trabecular bone in the femoral
1215 head of strepsirrhine primates. Journal of Human Evolution 43, 1-26.
1216 Ryan, T.M., Ketcham, R.A., 2005. Angular orientation of trabecular bone in the femoral head and its
1217 relationship to hip joint loads in leaping primates. Journal of Morphology 265, 249-263.
1218 Ryan, T.M., Krovitz, G.E., 2006. Trabecular bone ontogeny in the human proximal femur. Journal of
1219 Human Evolution 51, 591-602.
1220 Ryan, T.M., Walker, A., 2010. Trabecular bone structure in the humeral and femoral heads of
1221 anthropoid primates. Anatomical Record 293, 719-729.
1222 Ryan, T.M., Shaw, C.N., 2012. Unique suites of trabecular bone features characterize locomotor
1223 behavior in human and non-human anthropoid primates. Plos One 7, e41037.
1224 Ryan, T.M., Shaw, C.N., 2013. Trabecular bone microstructure scales allometrically in the primate
1225 humerus and femur. Proceedings of the Royal Society B: Biological Sciences 280, 20130172.
1226 Ryan, T.M., Shaw, C.N., 2015. Gracility of the modern *Homo sapiens* skeleton is the result of
1227 decreased biomechanical loading. Proceedings of the National Academy of Sciences 112, 372-
1228 377.
1229 Saers, J.P.P, Cazorla-Bak, Y., Shaw, C.N., Stock, J.T., Ryan, T.M., 2016. Trabecular bone structural
1230 variation throughout the human lower limb. Journal of Human Evolution 97, 97-108.
1231 Saers, J.P.P., 2017. Ontogeny and functional adaptation of trabecular bone in the human foot. Ph.D.
1232 Dissertation, University of Cambridge.

1233 Saparin, P., Scherf, H., Hublin, J.-J., Fratzl, P., Weinkamer, R. 2011. Structural adaptation of
1234 trabecular bone revealed by position resolved analysis of proximal femora of different primates.
1235 The Anatomical Record 294, 55-67.
1236 Sarmiento, E. 1994. Terrestrial traits in the hands and feet of gorillas. American Museum Novitates
1237 3091, New York: American Museum of Natural History.
1238 Sarringhaus, L.A., MacLatchy, L.M., Mitani, J.C., 2014. Locomotor and postural development of wild
1239 chimpanzees. Journal of Human Evolution 66, 29-38.
1240 Scherf, H., Harvati, K., Hublin, J.-J., 2013. A comparison of proximal humeral cancellous bone of
1241 great apes and humans. Journal of Human Evolution 65, 29-38.
1242 Scherf, H., Tilgner, R., 2009. A new high-resolution computed tomography (CT) segmentation
1243 method for trabecular bone architectural analysis. American Journal of Physical Anthropology
1244 140, 39-51.
1245 Shaw, C.N., Stock, J.T., 2009a. Habitual throwing and swimming correspond with upper limb
1246 diaphyseal strength and shape in modern human athletes. American Journal of Physical
1247 Anthropology 140, 160-172.
1248 Shaw, C.N., Stock, J.T., 2009b. Intensity, repetitiveness, and directionality of habitual adolescent
1249 mobility patterns influence the tibial diaphysis morphology of athletes. American Journal of
1250 Physical Anthropology 140, 149-159.
1251 Shaw, C.N., Ryan, T.M., 2012. Does skeletal anatomy reflect adaptation to locomotor patterns?
1252 Cortical and trabecular architecture in human and nonhuman anthropoids. American Journal of
1253 Physical Anthropology 147, 187-200.
1254 Shaw, C.N., Stock, J.T., 2013. Extreme mobility in the Late Pleistocene? Comparing limb
1255 biomechanics among fossil *Homo*, varsity athletes and Holocene foragers. Journal of Human
1256 Evolution 64, 242-249.
1257 Shea, B.T. 1981. Relative growth of the limbs and trunk in the African apes. American Journal of
1258 Physical Anthropology 56, 179-201.
1259 Simkin, A., Ayalon, J., Leichter, I., 1987. Increased trabecular bone density due to bone-loading
1260 exercises in postmenopausal osteoporotic women. Calcified Tissue International 40, 59-63.

1261 Sinclar, K.D., Farnsworth, R.W., Pham, T.X., Knight, A.N., Bloebaum, R.D., Skedros, J.G., 2013.
1262 The artiodactyl calcaneus as a potential 'control bone' cautions against simple interpretations of
1263 trabecular bone adaptation in the anthropoid femoral neck. Journal of Human Evolution 64, 366-
1264 379.
1265 Skedros, J.G., Hunt, K.J., Bloebaum, R.D., Relationships of loading history and structural and
1266 material characteristics of bone: development of the mule deer calcaneus. Journal of Morphology
1267 259, 281-307.
1268 Skerry, T., Lanyon, L., 1995. Interruption of disuse by short-duration walking exercise does not
1269 prevent bone loss in the sheep calcaneus. Bone 16, 269-274.
1270 Soames, R.W., 1985. Foot pressure patterns during gait. Journal of Biomedical Engineering 7, 120-
1271 126.
1272 Stern, J.T., Susman, R.L., 1983. The locomotor anatomy of *Australopithecus afarensis*. American
1273 Journal of Physical Anthropology 60, 279-317.
1274 Stern, J.T. 2000. Climbing to the top: A personal memoir of *Australopithecus afarensis*. Evolutionary
1275 Anthropology 9, 113-133.
1276 Stokes, I.A., Hutton, W.C., Stott, J.R., 1979. Forces acting on the metatarsals during normal walking.
1277 Journal of Anatomy 129, 579-590.
1278 Su, A., Carlson, K.J., 2017. Comparative analysis of trabecular bone structure and orientation in
1279 South African hominin tali. Journal of Human Evolution 106, 1-18.
1280 Sugiyama, T., Price, J.S., Lanyon, L.E., 2010. Functional adaptation to mechanical loading in both
1281 cortical and cancellous bone is controlled locally and is confined to the loaded bones. Bone 46,
1282 314-321.
1283 Susman, R.L., 1983. Evolution of the human foot - evidence from Plio-Pleistocene hominids. Foot
1284 and Ankle 3, 365-376.
1285 Susman, R L., Stern, J.T., Jungers, W.L. 1984. Arboreality and bipedality in the Hadar hominids.
1286 Folia Primatologica 43, 113-156.
1287 Susman, R.L., Brain, T.M., 1988. New first metatarsal (SKX 5017) from Swartkrans and the gait of
1288 *Paranthropus robustus.* American Journal of Physical Anthropology 77, 7-15.

1289 Susman, R.L., de Ruiter, D.J., 2004. New hominin first metatarsal (SK 1813) from Swartkrans.
1290 Journal of Human Evolution 47, 171-181.
1291 Sutherland, D.H., Olshen, R., Cooper, L., Woo, S.L., 1980. The development of mature gait. Gait and
1292 Posture 6, 163-170.
1293 Swartz, S., Parker, A., Huo, C. 1998. Theoretical and empirical scaling patterns and topological
1294 homology in bone trabeculae. Journal of Experimental Biology 201, 573-590.
1295 Thorpe, S.K.S., Crompton, R.H., 2005. Locomotor ecology of wild orangutans (*Pongo pygmaeus*
1296 *abelii*) in the Gunung Leuser ecosystem, Sumatra, Indonesia: A multivariate analysis using log-
1297 linear modelling. American Journal of Physical Anthropology 127, 58-78.
1298 Tocheri, M.W., Solhan, C.R., Orr, C.M., Femiani, J., Frohlich, B., Groves, C. P., Harcourt-Smith,
1299 W.E., Richmond, B.G., Shoelson, B., Jungers, W.L., 2011. Ecological divergence and medial
1300 cuneiform morphology in gorillas. Journal of Human Evolution 60, 171-184.

1301 Trinkaus, E. 1983. Functional-aspects of Neandertal pedal remains. Foot and Ankle 6, 377-390.

1302 Tsegai, Z.J., Kivell, T.L., Gross, T., Nguyen, N.H., Pahr, D.H., Smaers, J.B., Skinner, M.M., 2013.
1303 Trabecular bone structure correlates with hand posture and use in hominoids. Plos One 8,
1304 e78781.
1305 Tsegai, Z.J., Skinner, M.M., Gee, A.H., Pahr, D.H., Treece, G.M., Hublin, J.-J., Kivell, T.L., 2017.
1306 Trabecular and cortical bone structure of the talus and distal tibia in *Pan* and *Homo*. American
1307 Journal of Physical Anthropology 163, 784-805.
1308 Tuttle, R.H., 1969. Quantitative and functional studies on the hands of the Anthropoidea. I. The
1309 Hominoidea. Journal of Morphology 128, 309-363.
1310 Tuttle, R.H. 1981. Evolution of hominid bipedalism and prehensile capabilities. Philosophical
1311 Transactions of the Royal Society B 292, 89-94.
1312 Tuttle, R.H., Rogers, C.M., 1966. Genetic and selective factors in reduction of the hallux in *Pongo*
1313 *pygmaeus*. American Journal of Physical Anthropology 24, 191-198.

1314 Vereecke, E., D'Août, K., Clercq, D.D., Elsacker, L.V., Aerts, P., 2003. Dynamic plantar pressure
1315 distribution during terrestrial locomotion of bonobos (*Pan paniscus*). American Journal of
1316 Physical Anthropology 120, 373-383.
1317 Vernon, D.S., 2013. A morphometric analysis of the phalanges and a fragmentary first metatarsal
1318 from the Drimolen hominin site, South Africa. MPhil Dissertation, University of Johannesburg.
1319 Wallace, I.J., Kwaczala, A.T., Judex, S., Demes, B., Carlson, K.J., 2013. Physical activity
1320 engendering loads from diverse directions augments the growing skeleton. Journal
1321 of Musculoskeletal and Neuronal Interactions 13, 283-288.
1322 Ward, C.V., 2002. Interpreting the posture and locomotion of *Australopithecus afarensis*: Where do
1323 we stand? American Journal of Physical Anthropology 119, 185-215.
1324 Ward, C.V., Kimbel, W.H. and Johanson, D.C., 2011. Complete fourth metatarsal and arches in the
1325 foot of *Australopithecus afarensis*. Science 331, 750-753.

1326 White, T.D., Suwa, G., Asfaw, B. 1994. *Australopithecus ramidus*, a new species of early hominid
1327 from Aramis, Ethiopia. Nature 371, 306-312.

1328 White, T.D., Lovejoy, C.O., Asfaw, B., Carlson, J.P., Suwa, G. 2015. Neither chimpanzee nor human,
1329 *Ardipithecus* reveals the surprising ancestry of both. Proceedings of the National Academy of
1330 Sciences 112, 4877-4884.
1331 Whitehouse, W.J., 1974. The quantitative morphology of anisotropic trabecular bone. Journal of
1332 Microscopy-Oxford 101, 153-168.
1333 Wickham, H. 2009. ggplot2: Elegant Graphics for Data Analysis. New York: Springer-Verlag.
1334 Wood, B., Constantino, P. 2007. *Paranthropus boisei*: Fifty years of evidence and analysis. American
1335 Journal of Physical Anthropology 134, 106-132.
1336 Wunderlich, R.E., Ischinger, S.B., 2017. Foot use during vertical climbing in chimpanzees (*Pan*
1337 *troglodytes*). Journal of Human Evolution 109, 1-10.
1338 Zeininger, A., Patel, B.A., Zipfel, B., Carlson, K.J., 2016. Trabecular architecture in the StW 352
1339 fossil hominin calcaneus. Journal of Human Evolution 97, 145-158.

Zeininger, A., Schmitt, D., Jensen, J.L., Shapiro, L.J., Ontogenetic changes in foot strike pattern and calcaneal loading during walking in young children. Gait and Posture 59, 18-22.

Zipfel, B., Kidd, R.S., 2006. Hominin first metatarsals (SKX 5017 and SK 1813) from Swartkrans: A morphometric analysis. Homo 57, 117-131.

Zipfel, B., DeSilva, J. M., Kidd, R.S. 2009. Earliest complete hominin fifth metatarsal—implications for the evolution of the lateral column of the foot. American Journal of Physical Anthropology 140, 532-545.

Zipfel, B., DeSilva, J.M., Kidd, R.S., Carlson, K.J., Churchill, S.E., Berger, L.R., 2011. The foot and ankle of *Australopithecus sediba*. Science 333, 1417-1420.

Figures and tables

Table 1. Study sample composition

Taxon	Side (R/L)	Sex (M/F/?)	Locomotor mode
Pongo pygmaeus	6 (3/3)	1/4/1	Suspensory (torso-orthogrady)
Gorilla gorilla	10 (6/4)	5/5/0	Arboreal/ terrestrial knuckle-walker
Pan troglodytes	10 (5/5)	6/4/0	Arboreal/ terrestrial knuckle-walker
Homo sapiens	11 (9/2)	6/5/0	Bipedal
Paranthropus robustus (?) SKX 5017	(0/1)		Bipedal/arboreal (?)
SK 1813 (Hominin indet.)	(1/0)		Bipedal/arboreal (?)

Table 2. Results from reduced major axis regression analysis. Displayed are all trabecular paramaters analyzed and their relationship to size. Included are bone volume fraction (BV/TV), trabecular thickness (Tb. Th.), trabecular spacing (Tb. Sp.), trabecular number (Tb. N.), and degree of anisotropy (DA). CL- and CL+ represent confidence limits for 95% intervals, and results indicate positive versus negative size-related correlation. (*) Asterisks denote that the isometric slope is contained within the CLs, and isometric scaling cannot be rejected.

	variable	Isometric slope value	slope	CL -	CL +	*y*-int	R^2	*p*-value	result
Pongo									
	BV/TV	0	1.94	0.66	5.69	-6.61	0.13	0.48	+
	Tb.Th	1	1.27	0.44	3.62	-4.97	0.18	0.39	+
	Tb.Sp	1	-1.28	-3.81	-0.43	3.14	0.09	0.56	-
	Tb.N	0	0.54	0.18	1.68	-1.39	0.01	0.88	+
	DA	0	1.40	0.45	4.31	-5.28	0.01	0.84	+
Gorilla									
	BV/TV	0	0.89	0.43	1.81	-3.96	0.09	0.40	+
	Tb.Th	1	1.18	0.70	1.98	-5.05	0.56	**0.01**	+*
	Tb.Sp	1	1.43	0.69	2.98	-4.89	0.03	0.62	+*
	Tb.N	0	-0.99	-1.91	-0.51	3.17	0.24	0.16	-
	DA	0	1.15	0.63	2.11	-4.89	0.37	0.06	+
Pan									
	BV/TV	0	-1.42	-2.90	-0.69	3.35	0.08	0.42	-
	Tb.Th	1	1.87	0.92	3.79	-7.13	0.12	0.33	+*
	Tb.Sp	1	3.21	1.90	5.41	-10.39	0.55	**0.01**	+
	Tb.N	0	-2.10	-3.74	-1.18	6.66	0.44	**0.04**	-
	DA	0	1.25	0.59	2.63	-4.90	<0.01	0.94	+
Homo									
	BV/TV	0	2.74	1.37	5.49	-10.42	<0.01	0.82	+
	Tb.Th	1	1.41	0.72	2.75	-6.17	0.08	0.39	+*
	Tb.Sp	1	2.56	1.28	5.13	-8.92	<0.01	0.85	+
	Tb.N	0	-1.84	-3.67	-0.92	6.23	0.01	0.78	-
	DA	0	1.26	0.65	2.41	-5.07	0.14	0.26	+

1386 **Table 3. Summary statistics for all analyzed parameters and taxa.**

		Pongo pygmaeus	*Gorilla gorilla*	*Pan troglodytes*	SKX 5017	SK 1813	*Homo sapiens*
	BV/TV						
Head	Mean	0.32 ± 0.07	0.35 ± 0.05	0.38 ± 0.02	0.41	0.36	0.29 ± 0.04
	Range	0.19 - 0.23	0.28 - 0.421	0.29 - 0.44			0.23 - 0.34
	CV	22.70	13.10	13.40			15.50
Base	Mean	0.32 ± 0.09	0.33 ± 0.02	0.35 ± 0.03	0.38		0.24 ± 0.05
	Range	0.252- 0.47	0.28 - 0.37	0.31 - 0.40			0.16 - 0.33
	CV	26.80	7.00	7.80			30.00
	DA						
Head	Mean	0.24 ± 0.03	0.30 ± 0.04	0.33 ± 0.04	0.27	0.20	0.40 ± 0.04
	Range	0.19 - 0.28	0.25 - 0.35	0.27 - 0.39			0.33 - 0.46
	CV	13.10	12.80	12.60			9.00
Base	Mean	0.28	0.33 ± 0.04	0.37 ± 0.02	0.37		0.40 ± 0.04
	Range	0.19 - 0.34	0.25 - 0.40	0.35 - 0.41			0.34 - 0.45
	CV	18.50	13.00	5.30			8.90
	Trabecular thickness (mm)						
Head	Mean	0.26 ± 0.04	0.31 ± 0.04	0.29 ± 0.04	0.30	0.26	0.24 ± 0.02
	Range	0.20 - 0.31	0.26 - 0.37	0.22 - 0.34			0.20 - 0.29
	CV	16.90	12.00	14.00			10.50
Base	Mean	0.24 ± 0.04	0.28 ± 0.04	0.23 ± 0.02	0.25		0.20 ± 0.02
	Range	0.21 - 0.31	0.22 - 0.34	0.19 - 0.26			0.17 - 0.24
	CV	14.60	14.00	10.10			9.80
	Trabecular number (mm^{-1})						
Head	Mean	1.08 ± 0.07	0.88 ± 0.12	1.05 ± 0.20	1.15	1.32	1.13 ± 0.13
	Range	1.02 - 1.21	0.72 - 1.03	0.80 - 1.44			0.97 - 1.39
	CV	6.30	14.00	19.70			11.40
Base	Mean	1.21 ± 0.09	1.11 ± 0.11	1.39 ± 0.12	1.32		1.24 ± 0.17
	Range	1.11 - 1.34	0.99 - 1.34	1.23 - 1.58			0.91 - 1.51
	CV	7.60	9.70	8.90			13.60
	Trabecular spacing (mm)						
Head	Mean	0.70 ± 0.11	0.91 ± 0.20	0.75 ± 0.21	0.57	0.50	0.66 ± 0.10
	Range	0.53	0.69 - 1.19	0.48 - 1.12			0.49 - 0.82
	CV	15.80	22.00	28.10			14.90
Base	Mean	0.58 ± 0.09	0.63 ± 0.05	0.49 ± 0.05	0.50		0.63 ± 0.14
	Range	0.45 - 0.66	0.53 - 0.71	0.43 - 0.57			0.48 - 0.93
	CV	15.00	8.20	9.40			21.80

1387

1388

Table 4. Results from Kruskal-Wallis post hoc tests in interspecies BV/TV and DA ratio. Values above grey boxes represent the head and values below grey boxes represent the base.

	Pongo	*Gorilla*	*Pan*	*Homo*
BV/TV				
Pongo		0.029	0.560	<0.001
Gorilla	1.000		1.000	<0.001
Pan	1.000	1.000		<0.001
Homo	<0.001	<0.001	<0.001	
DA				
Pongo		1.000	1.000	1.000
Gorilla	0.045		1.000	1.000
Pan	0.252	1.000		0.690
Homo	1.000	0.214	1.000	

Table 5. Kruskal-Wallis post hoc test of interspecies absolute DA values. Values above grey diagonal boxes represent head, values below represent the base.

	Pongo	*Gorilla*	*Pan*	*Homo*
Pongo		0.096	<0.01	<0.001
Gorilla	0.707		0.993	<0.001
Pan	<0.01	<0.05		<0.01
Homo	<0.01	<0.01	0.910	

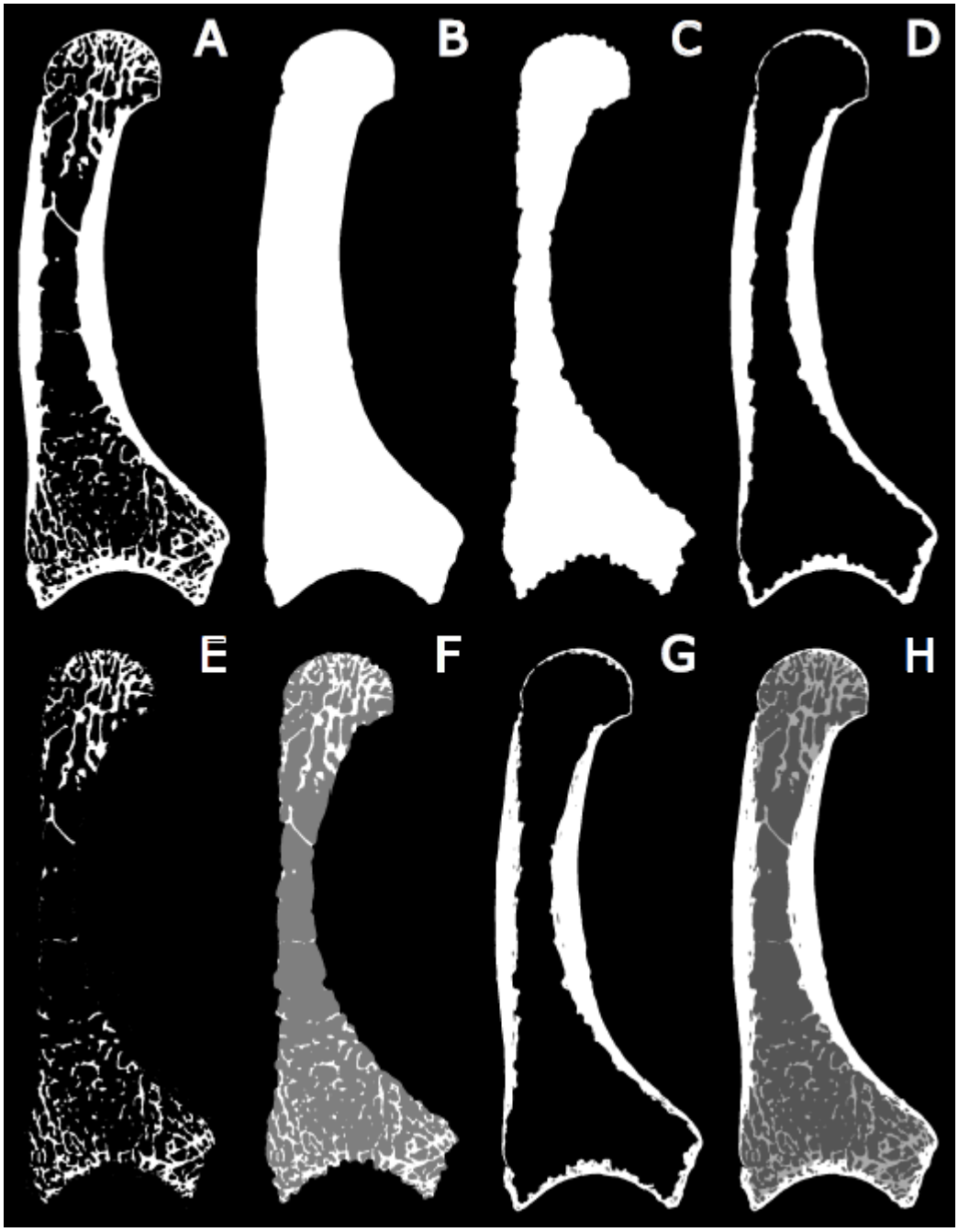

Figure 1. Masking procedure used to segment different components of bone. Illustrated here is a *Gorilla* first metatarsal that has undergone complete segmentation. From left to right: (a) segmented image; (b) outer mask; (c) inner mask; (d) cortical mask; (e) trabeculae only image; (f) MaskSeg In; (g) MaskSeg Out; (h) MaskSeg (this is the mask which is used for trabecular quantification by medtool).

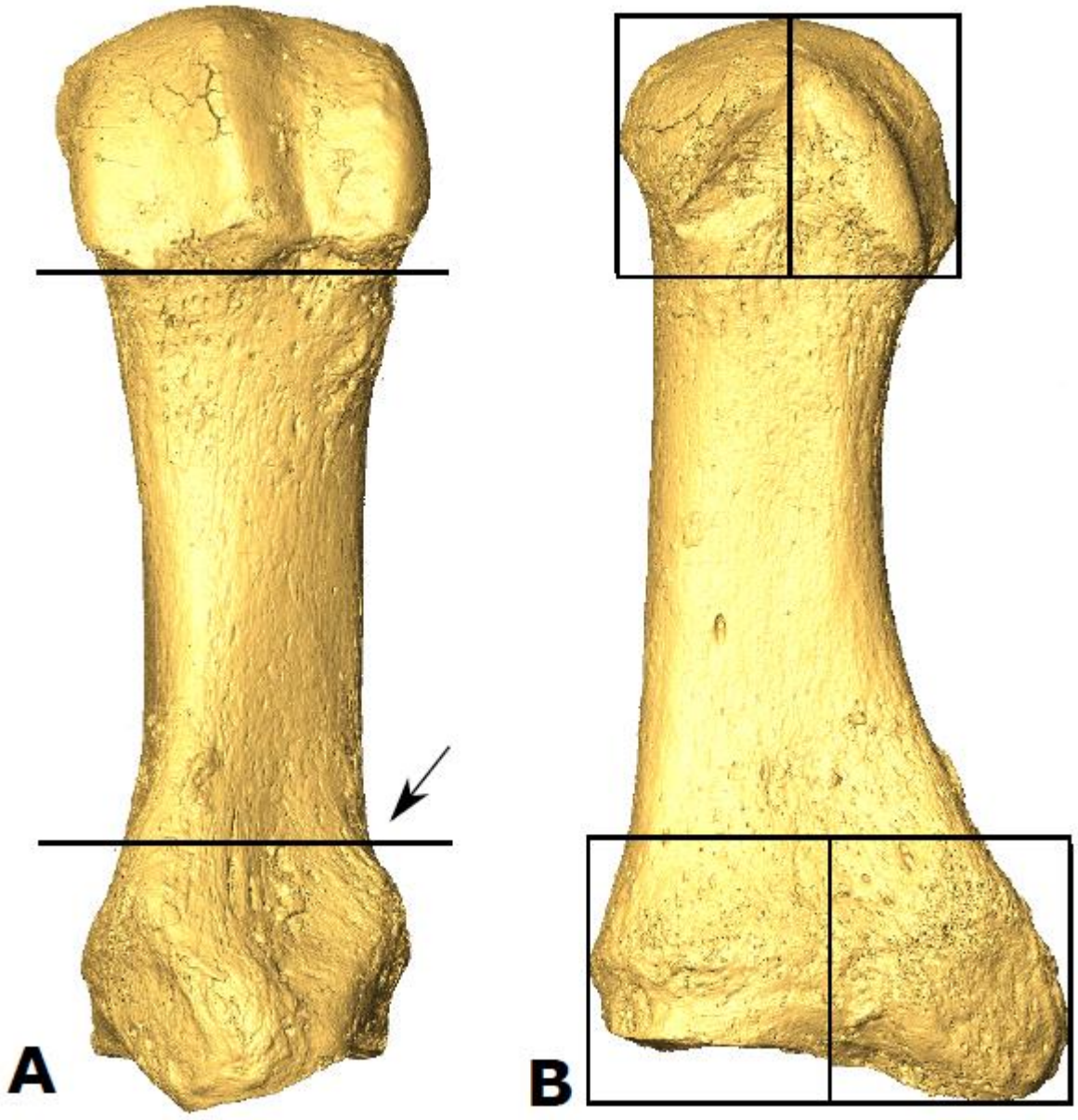

Figure 2. Delineation of the epiphyses and the dorsal and plantar sections. (a) The head was delineated where the articular surface terminates on the plantar aspect of the bone. Proximally, the base was delineated based on a homologous curvature on the medial aspect of the shaft (indicated by the arrow). (b) Both the base and the head were separated into dorsal and plantar sections by dividing in half the maximum dorso-plantar width.

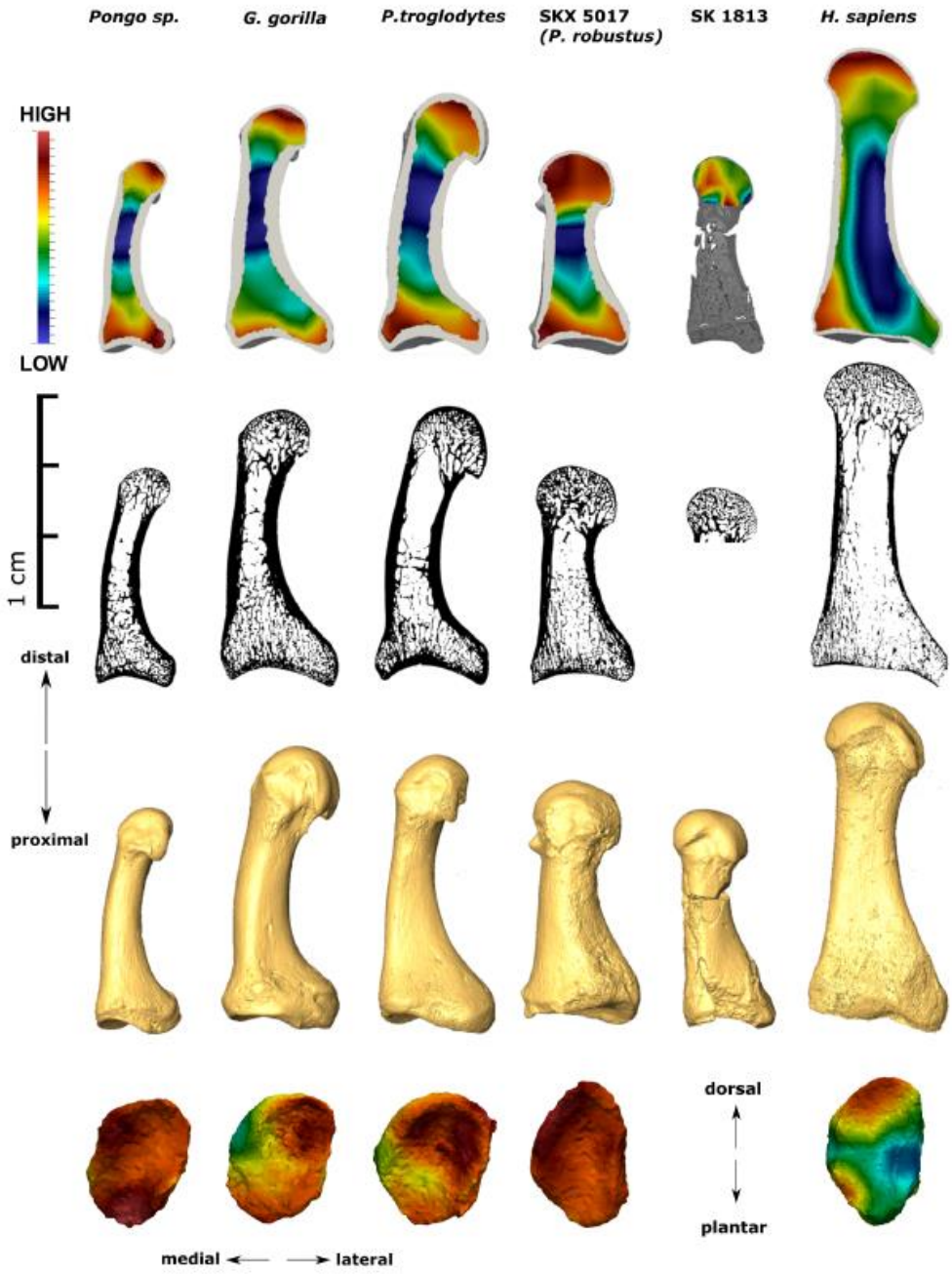

Figure 3. Representative specimens from each taxon. From top to bottom: BV/TV color maps of MT1 sagittal cross-section, segmented images, isosurfaces of external bone, and BV/TV color maps of proximal articular surfaces. BV/TV color maps are scaled to individual specimen ranges to visualize patterns of trabecular distribution as opposed to overall differences in BV/TV values. The first three rows are scaled to represent actual size differences between taxa. The color maps on the fourth row are all scaled to the same size, and do not represent natural size. SKX 5017 base on bottom row is mirrored to match the side of all other specimens.

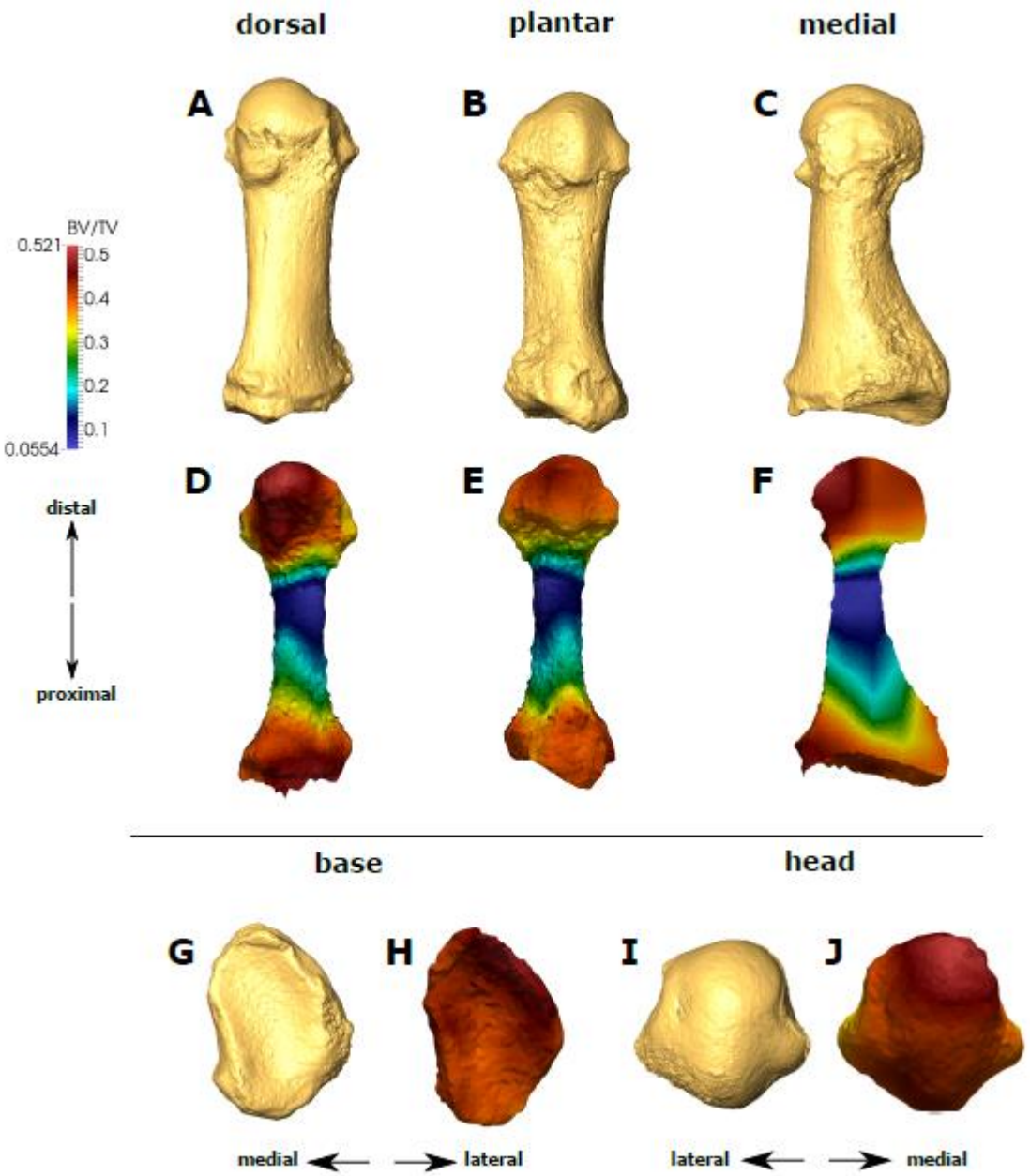

1432

1433 Figure 4. SKX 5017. Isosurfaces showing the external morphology of the element (a, b, c, g, i), and
1434 color maps of trabecular bone BV/TV (d, e, f, h, j). Images over the line show overall trabecular
1435 distribution throughout the whole bone in different positions, and images below the line display the
1436 dorso-plantar trabecular distribution in the epiphyses.

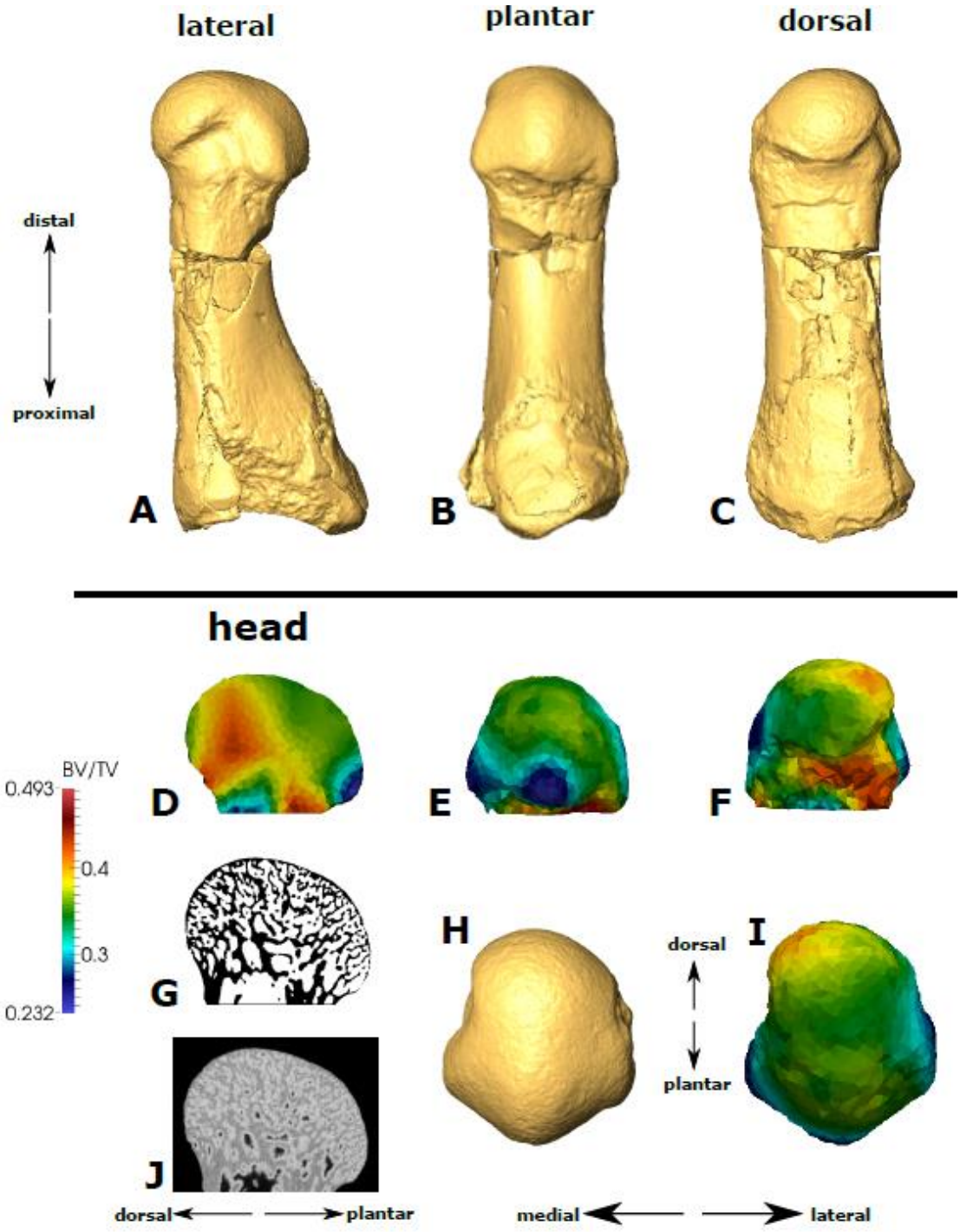

1437

1438 Figure 5. SK 1813. Isosurfaces showing the external morphology of the element (a, b, c, h). Images a,
1439 b, and c display the damage to the shaft and proximal aspect of the bone. Below the line are various
1440 visualizations of the metatarsal head. Illustrated are color maps of trabecular bone BV/TV (d, e, f, i).
1441 Notice the relatively dorsal position of high BV/TV, which is most clearly seen in the sagittal cross-
1442 section (d). This is also noticeable when viewing the element on its plantar (e), dorsal (f), and distal
1443 aspects (i). Also shown is the segmentation (g), and the original CT scan (j) of the head.

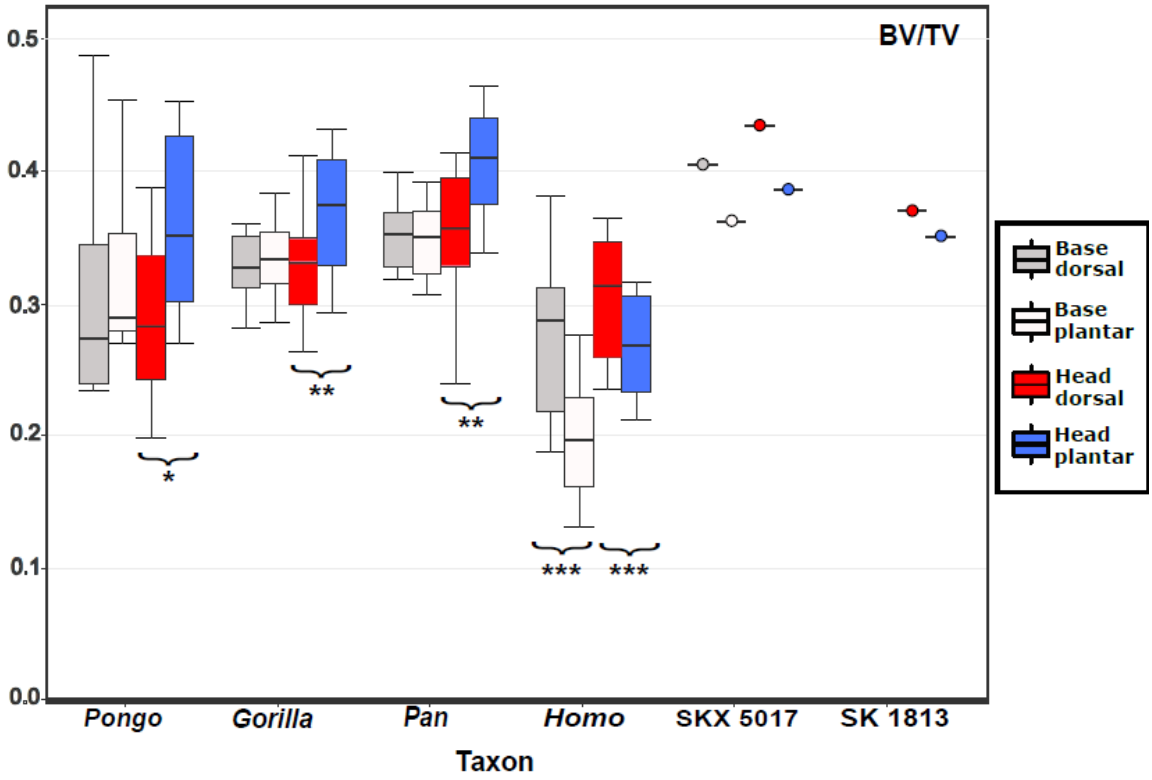

1444

1445 Figure 6. Boxplot showing raw BV/TV values within each analyzed region and each taxon.

1446 Significant differences in pairwise comparisons are denoted using asterisks [(*) = $p<0.05$; (**) =

1447 $p<0.005$; (***) = $p<0.001$)]. Within the base none of the non-human apes show significant differences

1448 between dorsal and plantar regions, whereas modern humans do. All taxa show significant differences

1449 between the dorsal and plantar regions of the head.

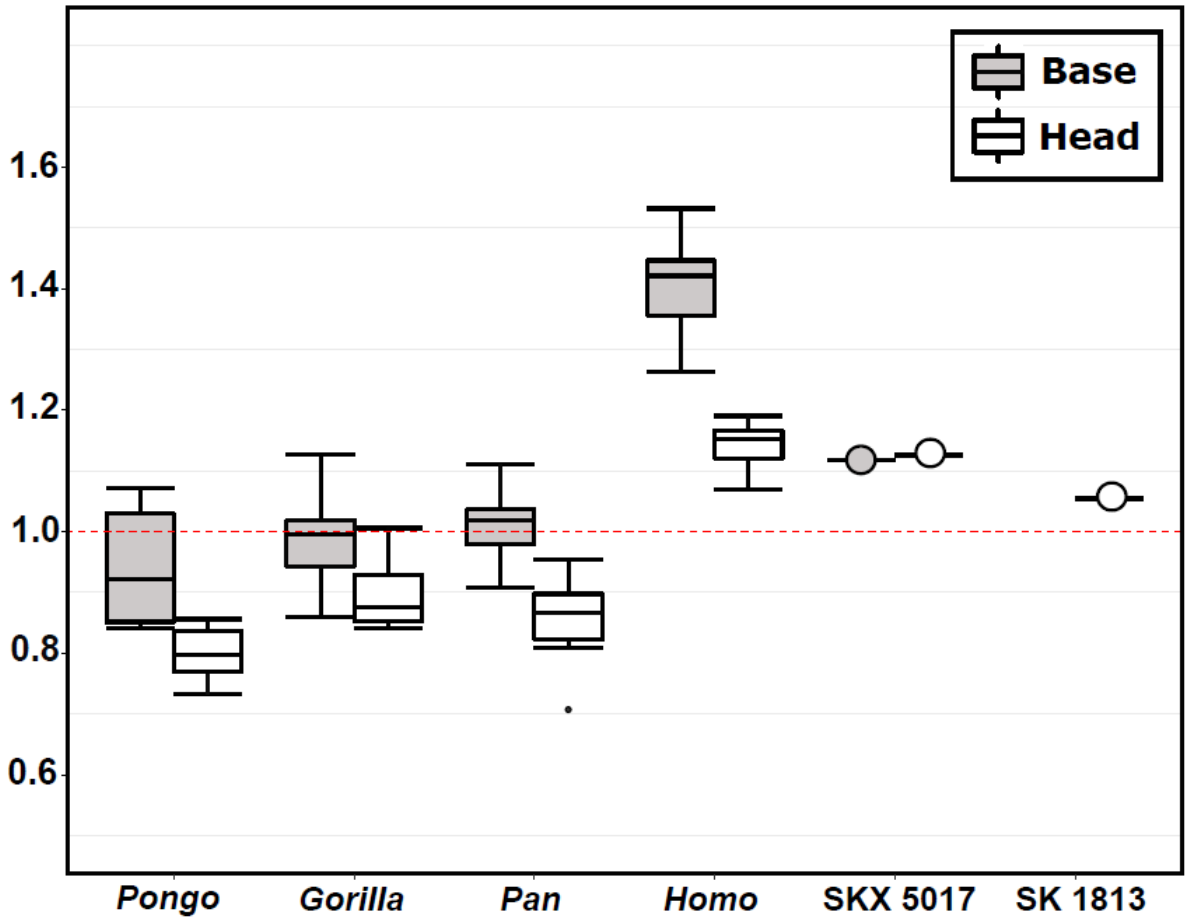

Figure 7. Boxplot of BV/TV ratio within the base and head of each taxon. Ratio represents the relative trabecular distribution; this is obtained by dividing dorsal values by plantar values and multiplying by 100. A ratio over one represents a more dorsal distribution and a ratio under one represents a more plantar distribution. Red dotted line represents an equal dorso-plantar distribution of trabecular bone.

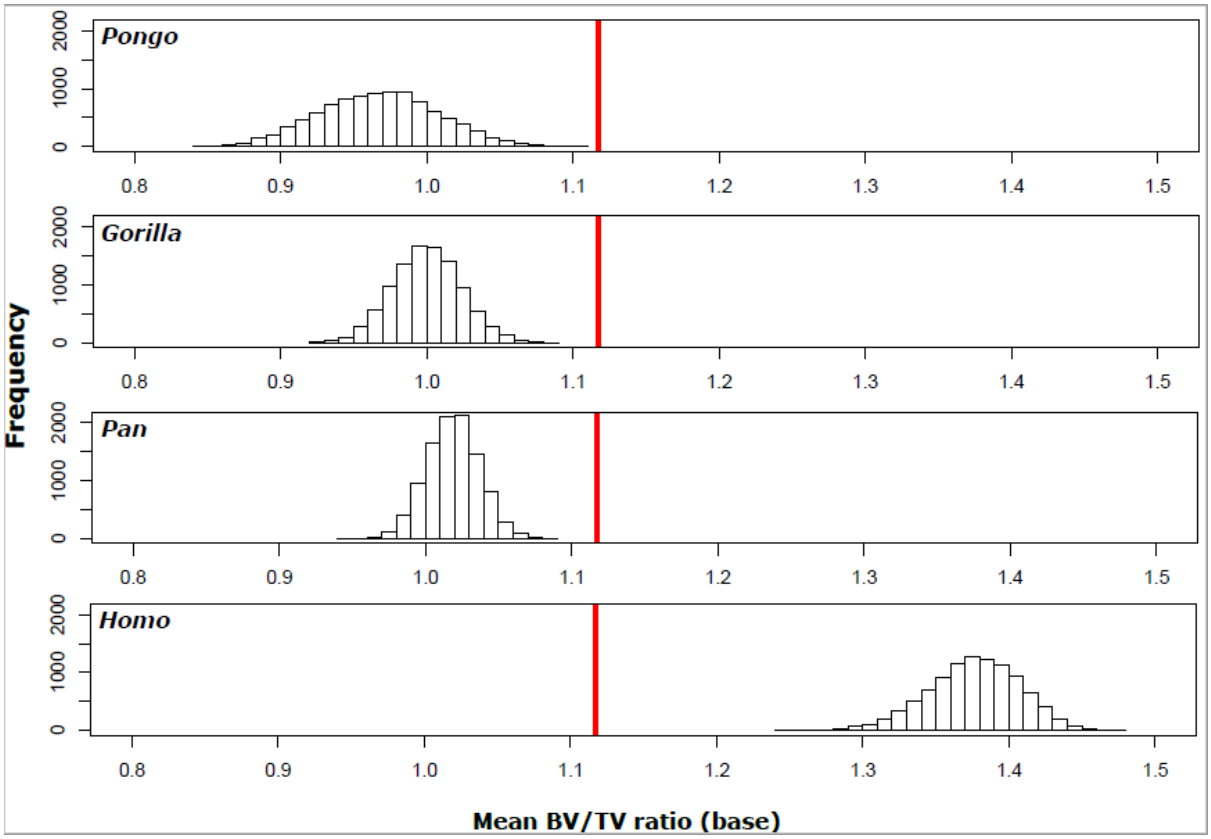

Figure 8. Bootstrap plots showing the resampled and redistributed sample means of BV/TV ratio within the base of each taxon. The red line represents the original BV/TV ratio of SKX 5017. Its position in the histograms represents the likelihood that the mean BV/TV ratio of the fossil hominins will fall within the range seen in modern taxa. In all cases, the red line falls outside the range of modern taxa.

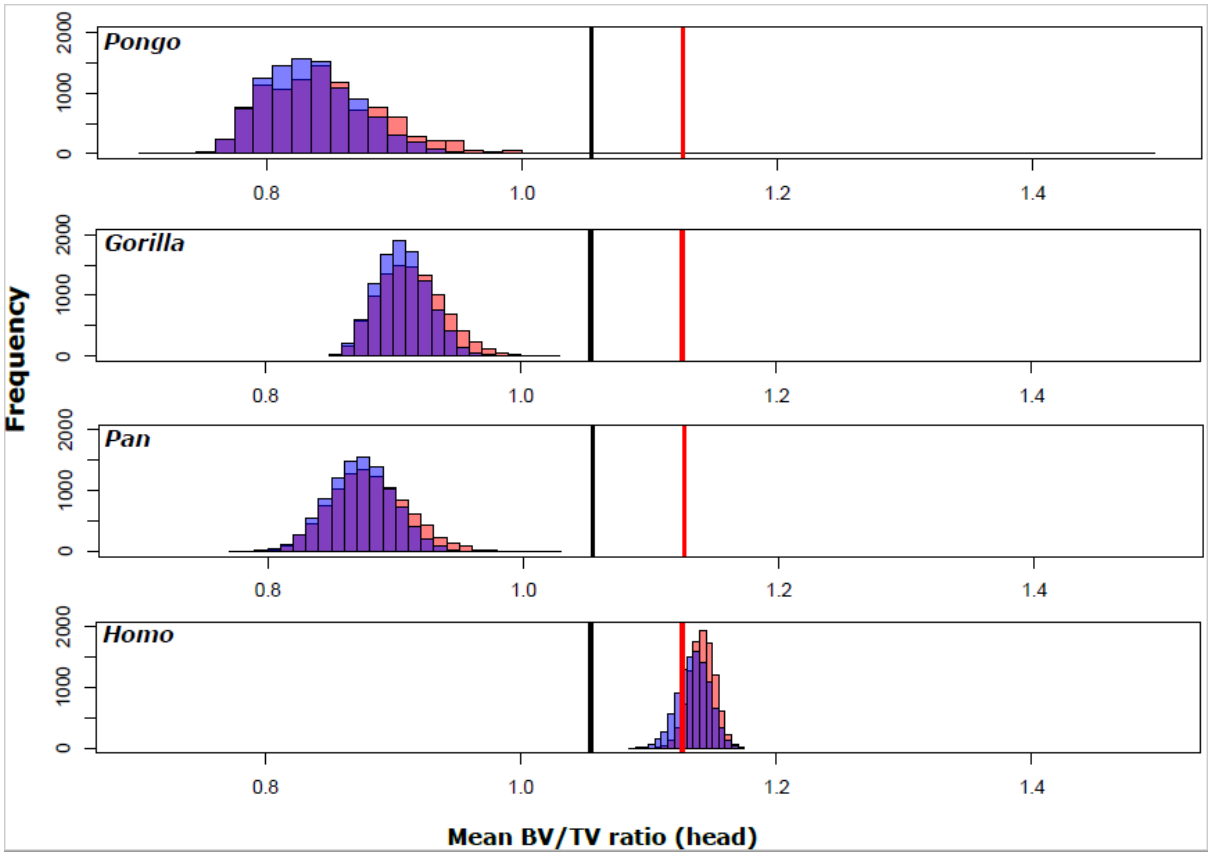

Figure 9. Bootstrap plots showing the sample means of BV/TV ratio within the head of each taxon. Pink bars represent the modern samples resampled and redistributed with SKX 5017; blue bars represent modern samples resampled and redistributed with SK 1813; purple bars represent overlap between the two samples. The red line represents the original BV/TV ratio of SKX 5017 and the black line represents the original BV/TV ratio of SK1813. The BV/TV ratio of SK 1813 falls outside the range of all taxa, with the exception of *Pongo*. The BV/TV ratio of SKX 5017 falls within the range of modern humans.

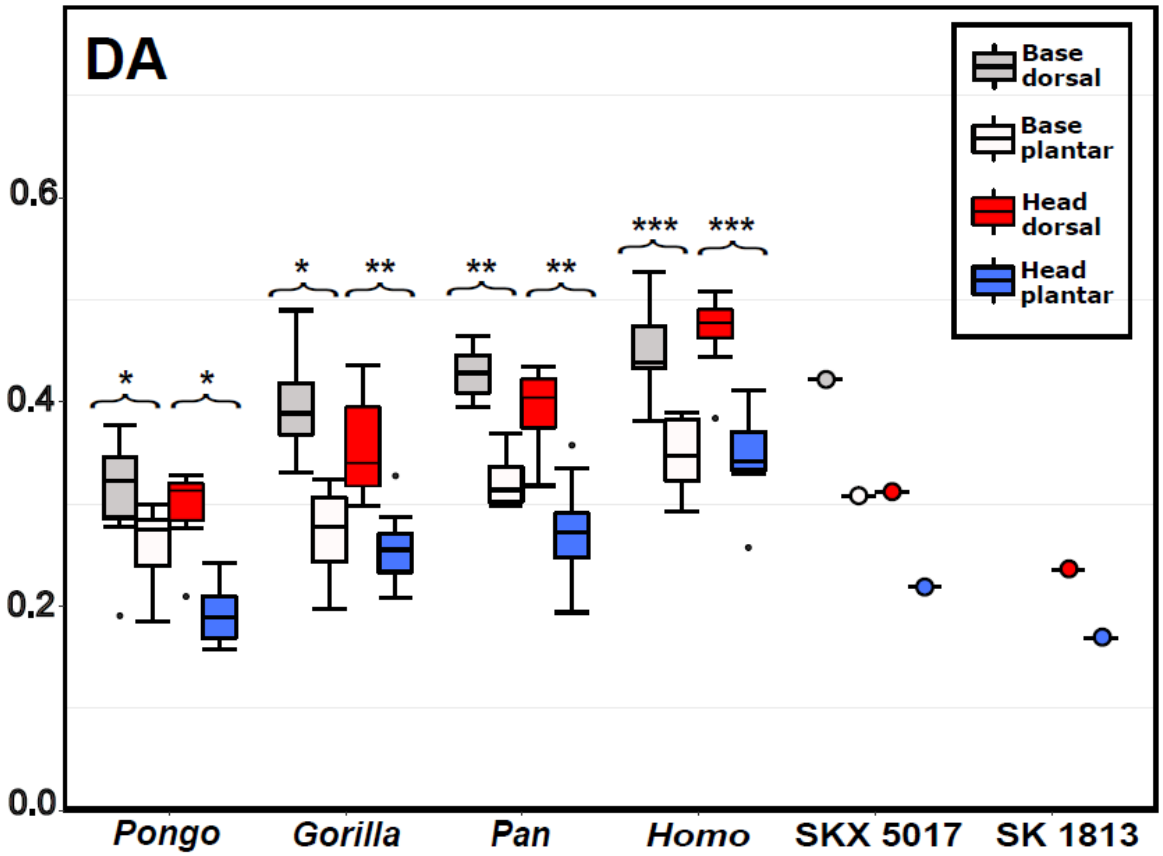

Figure 10. Boxplot showing raw DA values within each analysed region and each taxon. Significant differences in pairwise comparisons are denoted using asterisks (*) = $p<0.05$; (**) = $p<0.005$; (***) = $p<0.001$). All taxa display significantly higher DA in the dorsal regions of the element. Overall, modern humans show the absolute highest DA, and SK 1813 shows the lowest.

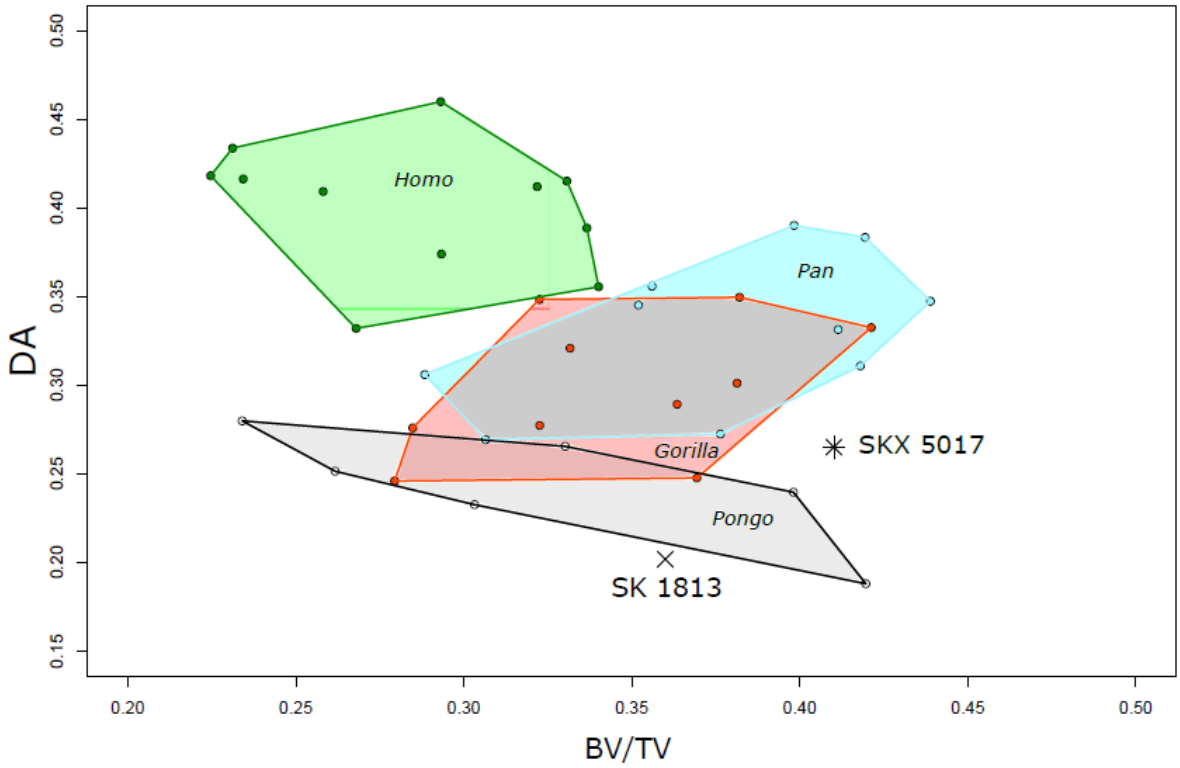

1474

1475 Figure 11. Scatterplot showing DA and absolute BV/TV values for the heads of all taxa. Dorsal and

1476 plantar regions have been combined to illustrate patterns in the entire epiphysis.

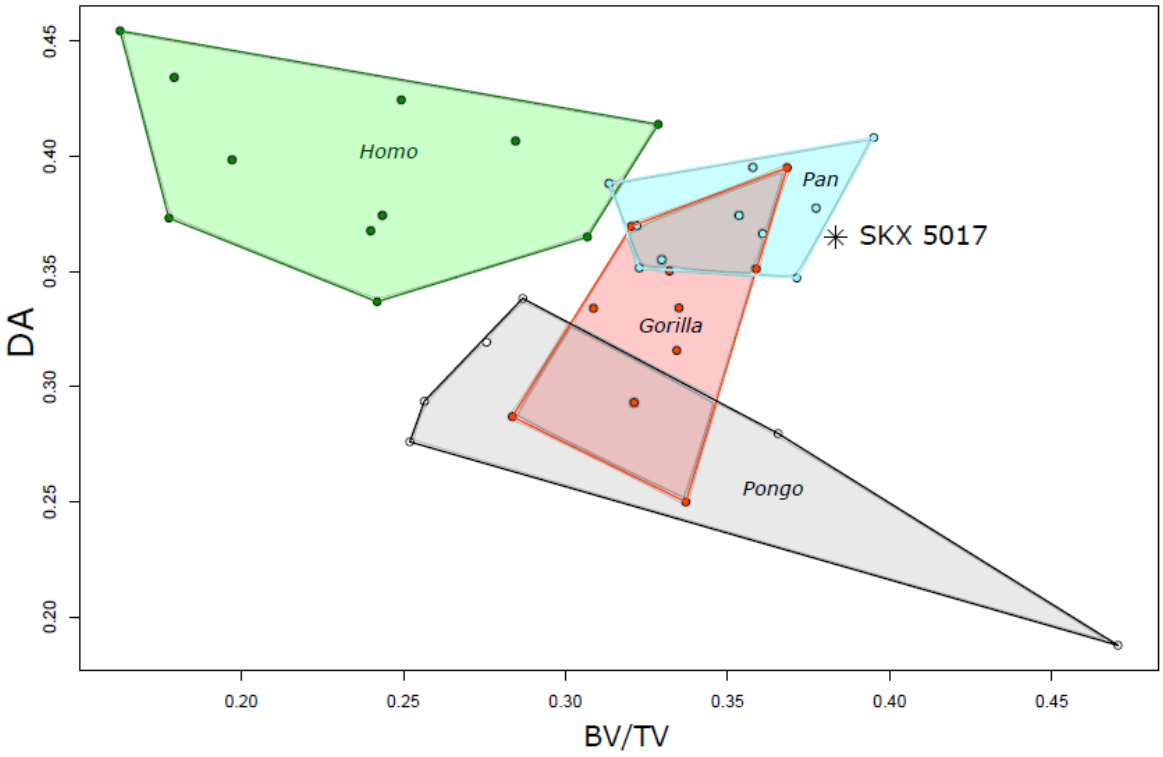

1477

1478 Figure 12. Scatterplot showing DA and absolute BV/TV values for the bases of all taxa. Dorsal and

1479 plantar regions have been combined to illustrate patterns in the entire epiphysis.

1480

1481

1482